islets. We clarified the problem of low efficiency of gene transduction in the inside of islets where β-cells exist, and we propose here a new strategy for efficient gene transfer to pancreatic β-cells by the direct injection of Ad vectors through the celiac artery *in vivo*.

2. Materials and methods

2.1. Ad vectors

Ad vectors were constructed by an improved *in vitro* ligation method [17,18]. Briefly, an *Escherichia coli* β-galactosidase (LacZ) and a green fluorescent protein (GFP) gene, derived from pCMVβ (Clontech, Palo Alto, CA) and pEGFP-N1 (Clontech), respectively, were inserted into pHMCA5 containing a CA promoter (a β-actin promoter/CMV enhancer/β-actin intron) [19], resulting in pHMCA-LacZ and pHMCA-GFP, respectively. These plasmids were then digested with I-*Ceu*I and PI-*Sce*I and ligated with I-*Ceu*I/PI-*Sce*I-digested pAdHM4 [17], resulting in pAdHM4-CALacZ and pAdHM4-CAGFP, respectively. Viruses were generated with the transfection of *Pac*I-digested pAdHM4-CALacZ and pAdHM4-CAGFP, respectively, into 293 cells with SuperFect (Qiagen, Valencia, CA) according to the manufacturer's instructions. Each virus, Ad-CALacZ and Ad-CAGFP, was purified by $CsCl_2$ gradient centrifugation and dialyzed with a solution consisting of 10 mM Tris (pH 7.5), 1 mM $MgCl_2$, and 10% glycerol. The virus particles and biological titer were determined by a spectrophotometrical method [20] and by using an Adeno-X Rapid Titer Kit (Clontech), respectively. The ratio of the biological-to-particle titer was 1:10 for both Ad-CALacZ and Ad-CAGFP.

2.2. Islet preparation

Islets of Langerhans were isolated from male C57/BL6 mice and Wistar rats by a collagenase digestion technique [21]. Isolated islets were washed with Krebs–Ringer bicarbonate buffer (KRBB; 129.4 mM NaCl, 5.2 mM KCl, 2.7 mM $CaCl_2$, 1.3 mM KH_2PO_4, 1.3 mM $MgSO_4$, and 24.8 mM $NaHCO_3$ (equilibrated with 5% CO_2/95% O_2, pH 7.4)) containing 2.8 mM glucose and cultured overnight (about 20 h) in RPMI 1640 medium containing 5.5 mM glucose and 10% fetal calf serum.

2.3. Ad vector-mediated gene transduction in vitro

Cultured islets were treated with each Ad vector at 2×10^9 vector particle (VP)/100–200 islets for 1 h with or without preincubation in Ca^{2+}-free KRBB containing 5.5 mM glucose, 1 mM EGTA, and 0.2% bovine serum albumin for 15 min. Then, the medium containing the vectors was removed and fresh medium was added to the islets. Twenty-four hours later, transgene expression in the islets was evaluated histologically and by luminescent assay using a Luminescent β-gal detection kit II (Clontech). The value of β-galactosidase activity was corrected with total islet protein contents.

2.4. Ad vector-mediated gene transduction in vivo

Male C57/BL6 mice and Wistar rats were anesthetized and subjected to laparotomy. The hepatic artery with the portal vein at the porta hepatis and the splenic artery at the hilum of the spleen were ligated, respectively. Then, the celiac artery branched from the abdominal aorta was dissected out from the surrounding connective tissue, and the upper side of the artery was clamped. After a 29-G needle was inserted into the lower side of the clamped point of the artery, 100 μl of Ad vector suspension at 1×10^{10} VP in PBS was injected (Fig. 3A). Five minutes later, the needle was pulled out and pancreatic islets were isolated. Isolated islets were cultured for 24 h before transgene expression was evaluated.

2.5. Histology

To determine LacZ expression, after 24 h of Ad-CALacZ transduction the islets were washed with PBS and fixed with 0.5% glutaraldehyde for 20 min, followed by washing with PBS. The whole islets were then stained with 5-bromo-4-chloro-3-indolyl-β-D-galactopyranoside (X-gal) for 2 h. For slices of islets, fixed islets were put into a warm solution of PBS containing 2% low melting agar and cooled in a refrigerator. Solid pieces of agar gel including islets were then sunk in 20% sucrose in PBS and embedded in Tissue-Tek OCT compound (Sakura Finetek, Tokyo, Japan). Frozen sliced sections were prepared with a cryostat (Leica CM1850; Leica Microsystems, Wetzlar, Germany) and stained with X-gal for 2 h. In the case of GFP expression, after 24 h of Ad-CAGFP transduction GFP fluorescence in the islets was visualized via confocal microscopy (Leica TCS SP2 AOBS; Leica Microsystems). For sliced sections of islets, islets were fixed with 4% paraformaldehyde phosphate buffer solution for 10 min and washed with PBS, followed by preparing solid agar gel including islets as described above. Islet gel embedded in paraffin were sectioned, deparaffinized, and washed with Tris-buffered saline containing 0.1% Tween 20 (TBS-T). These sections were then incubated with a polyclonal guinea pig anti-swine insulin antibody (diluted to 1:2) (Dako, Kyoto, Japan) overnight for 4 °C, washed with TBS-T, and incubated with a rhodamine-labeled anti-rabbit IgG (diluted to 1:20) (Dako) for 30 min at room temperature. After sliced sections were mounted with coverslips, the fluorescence of GFP or rhodamine was determined using fluorescence microscopy (IX81; Olympus, Tokyo, Japan).

2.6. Western blotting

Islets were lysed in lysis buffer (25 mM Tris (pH 7.5), 150 mM NaCl, 5 mM EDTA, 1% Triton X-100, and 0.5% sodium deoxycholate) containing protease inhibitor cocktail (Sigma, St. Louis, MO). B16 cells stably expressing mouse coxsackievirus and adenovirus receptor (CAR) (B16CAR), which were constructed by the transfection of mouse CAR-expressing plasmid, and mouse β-cell line MIN6 cells were also lysed. Islet and cell lysates (15 μg) were subjected to SDS-PAGE on 12.5% polyacrylamide gel and transferred onto

nitrocellulose membranes (PROTRAN; Schleicher and Schuell, Dassel, Germany). After blocking with TBS-T supplemented with 5% nonfat dry milk for 1 h at room temperature, blotted membranes were incubated with a goat anti-mouse CXADR (CAR) antibody (R&D systems, Minneapolis, MN) in TBS-T containing 3% nonfat dry milk overnight at 4 °C, followed by washing with TBS-T. Membranes were then incubated with a horseradish peroxidase-conjugated anti-goat IgG (Chemicon, Temecula, CA) in TBS-T containing 3% nonfat dry milk for 2 h at room temperature, washed, and visualized by chemiluminescence using ECL Plus Western blotting detection reagents (Amersham Bioscience, Piscataway, NJ). For the detection of an internal control, a monoclonal anti-β-actin antibody (Sigma) and a horseradish peroxidase-linked anti-mouse IgG (Cell Signaling Technology, Beverly, MA) were used.

3. Results and discussion

Ad requires CAR on the cell surface as a primary receptor for infection, and its genome persists episomally in host cells [10,11,22]. First, we examined the expression of CAR in both fresh and cultured pancreatic islets by Western blotting analyses. As shown in Fig. 1A, we found that fresh mouse pancreatic islets expressed CAR, and its expression was enhanced in 20 hours-cultured islets. We then examined the efficiency of Ad vector-mediated gene expression using overnight-cultured islets. Mouse Islets were transduced with Ad-CALacZ, and β-galactosidase expression was evaluated by X-gal staining. As shown in Fig. 1B, whole islet staining showed high levels of β-galactosidase expression in the entire islet of not only mice but rats. However, X-gal staining of sliced sections of islets revealed β-galactosidase expression only in the periphery of the islet of both mice and rats. A similar pattern of transgene expression was observed in confocal microscopic analyses of the islet transduced with Ad-CAGFP (Fig. 1C). The Ad vector-mediated gene expression increased in a dose-dependent manner (Fig. 1C and D). More enhancement of transgene expression was not observed in higher concentration than 2×10^9 VP (data not shown). These results suggested that CAR might be expressed in only peripheral cells of islets or that Ad might not be able to infect the cells in the inside of islets due to physical barrier by the cells.

Previously, we and others developed several types of fiber-modified Ad vectors, which mediate efficient gene transduction into the cells that express a very low level of CAR. Arg-Gly-Asp (RGD) peptide or 7-tandem lysine residues (K7) peptide, in targeting αv integrins or heparan sulfates of the cellular surface, respectively, was introduced in the fiber knob of Ad vector [23–27]. The efficiency of gene transduction was improved in various types of cells by these fiber-modified Ad vectors [27,28]. To investigate whether gene transduction into islets is enhanced using these fiber-modified Ad vectors, we measured the β-galactosidase expression in islets transduced with these Ad vectors by luminescence assay. Neither fiber-modified Ad vector containing RGD peptides nor that containing K7 peptides enhanced β-galactosidase activity of islets (data not shown). These findings suggest that transgene expression only in the periphery of islets is not due to the levels of CAR expression in islets, but to physical obstruction against Ad invasion into the inside of islets, though αv integrins and

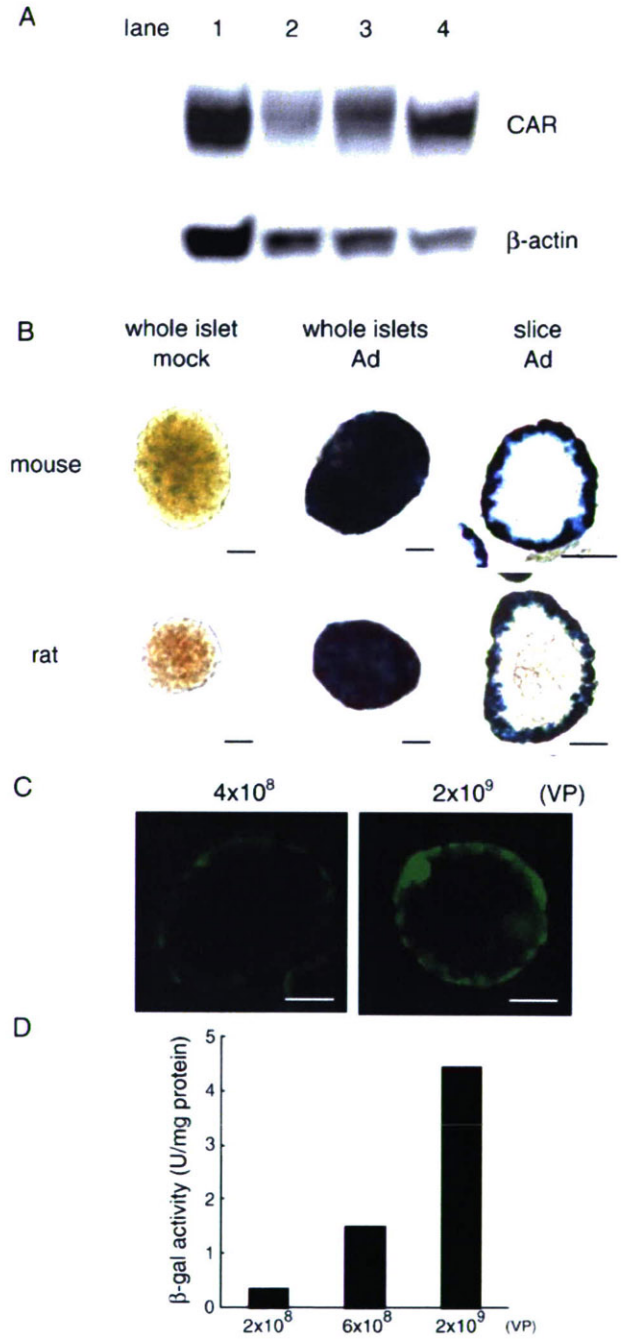

Fig. 1. Ad vector transduction into pancreatic islets *in vitro*. (A) Lysates of B16CAR (lane 1), fresh (lane 2), 20 hours-cultured (lane 3) mouse islets, and MIN6 cells (lane 4) were subjected to Western blotting using an anti-mouse CAR or anti-β-actin antibody. (B) Overnight-cultured islets of mice and rats were transduced with Ad-CALacZ for 1 h. The medium containing the Ad vector was exchanged for fresh medium, and X-gal staining was performed 24 h later. Bars represent 50 μm. (C) Mouse islets were transduced with Ad-CAGFP at 4×10^8 or 2×10^9 VP/100–200 islets for 1 h. Confocal microscopic analyses were performed 24 h later. Bars represent 50 μm. (D) Mouse islets were transduced with Ad-CALacZ at the indicated concentrations for 1 h. The β-galactosidase activity of the islets was measured by luminescence assay 24 h later.

heparin sulfates might not be expressed in the cells in the inside of islets. The fact of distinct CAR expression in mouse β-cell line MIN6 cells (Fig. 1A) also supports this assumption.

Transduction efficiency in fresh islets with the conventional Ad vector was equal to that in overnight-cultured islets (data not shown), suggesting that a low level of CAR expression in fresh islets would be enough for Ad infection. The reason why CAR expression in islets was enhanced by cultivation is unknown. Because it has been reported that CAR expression is enhanced by long term culture or influenced by culture medium in cardiomyocytes [29,30], same mechanism might work in islet cells. Ad vector-mediated gene expression *in vitro* lasts for a long term if the cells do not divide. Since islets do not proliferate *in vitro* and can be cultured for only a few days, gene expression would last throughout the duration of islet culture.

To overcome the physical problem of Ad infection into the cells in the inside of islets, we examined the effect of Ca^{2+}-free condition in which cell-to-cell adhesion becomes weak on Ad vector transduction into islets. Fig. 2A shows that preincubation in Ca^{2+}-free buffer for 15 min before transduction with Ad-CALacZ effectively enhanced β-galactosidase activity of islets. However, confocal microscopic analyses did not reveal distinct enhancement of transduction efficiency especially in the inside of islets (Fig. 2B). The Ca^{2+}-free treatment or collagenase digestion which makes cell-to-cell adhesion weak has a limitation because excessive treatments destroy the form of the islet.

Pancreatic islets are one of the most vascularized organs of the body. The density of the islet capillary network and blood flowing through the islets is about five times greater than that in exocrine pancreatic tissue [31,32]. This probably reflects the requirements of the islets for rich supplies of nutrients and oxygen, as well as for rapid disposal of metabolites and secreted hormones. We next tried Ad vector transduction through blood vessels that branch into the islet capillary network to obtain

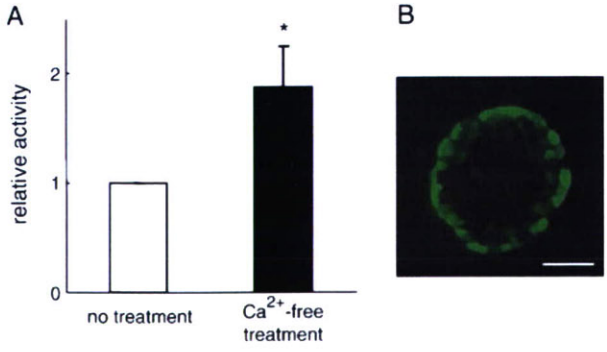

Fig. 2. Effect of Ca^{2+}-free treatment on Ad vector transduction into pancreatic islets. (A) Mouse islets were preincubated in Ca^{2+}-free KRBB for 15 min before they were transduced with Ad-CALacZ for 1 h. The medium containing the Ad vector was exchanged for fresh medium, and β-galactosidase activity of the islets was measured by luminescence assay 24 h later. The β-galactosidase activity was represented for a ratio to that of untreated islets. The data are expressed as the mean ± S.D. ($n=3$). Statistical significance was evaluated by unpaired Student's t test. $*p<0.05$ vs. no treatment. (B) Mouse islets were preincubated in Ca^{2+}-free KRBB for 15 min before they were transduced with Ad-CAGFP for 1 h. Confocal microscopic analyses were performed 24 h later. A bar represents 50 μm.

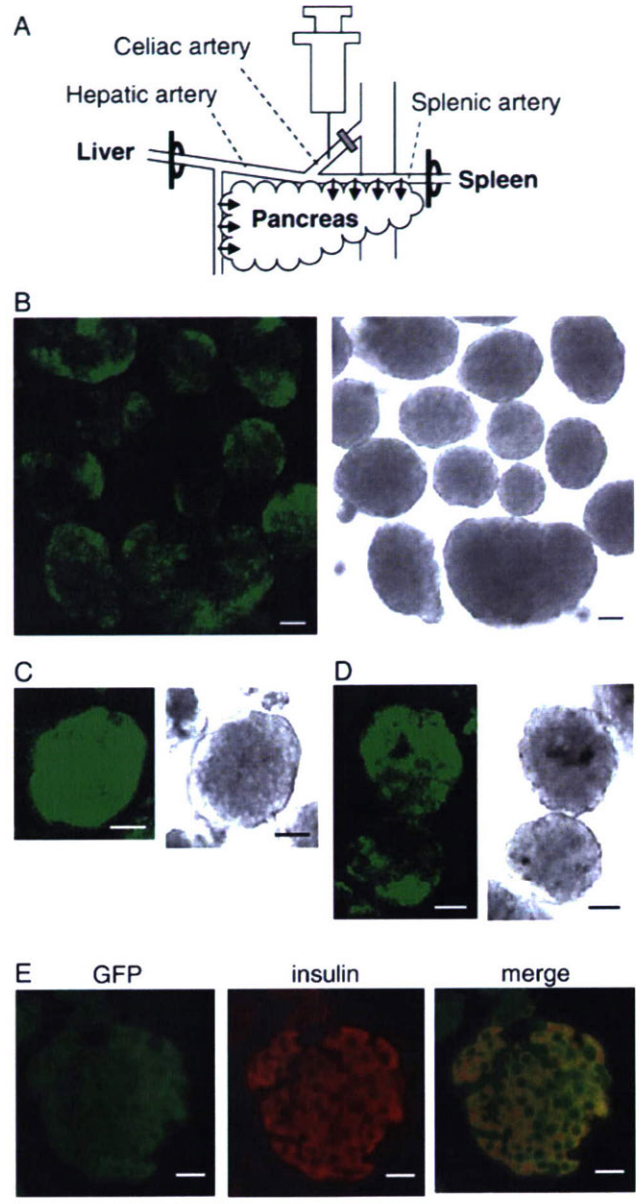

Fig. 3. Ad vector transduction into pancreatic islets *in vivo*. (A) Schema of Ad vector transduction *in vivo*. After ligation of the hepatic artery with the portal vein at the porta hepatis and the splenic artery at the hilum of the spleen, respectively, Ad-CAGFP was injected into the lower side of the clamed point of the celiac artery. Five minutes later, pancreatic islets were isolated and cultured for 24 h. (B–D) Confocal microscopic analyses of pancreatic islets of mice (B, C) and rats (D). An islet expressing GFP throughout the islet (C) was also observed. Each left panel and right panel represents the image of GFP-expressing islets and the corresponding visible image, respectively. Bars represent 50 μm. (E) Immunohistochemical analyses of sliced sections of mouse islets. Paraffin sections of islets were stained using an anti-insulin antibody and visualized with rhodamine. Bars represent 50 μm.

more efficient gene transduction, especially into the inside of islets. The celiac artery branched from the abdominal aorta is upper and proximal vessel toward the pancreas (Fig. 3A). After ligation of the hepatic artery with the portal vein and the splenic artery, respectively, Ad-CAGFP was injected through the celiac artery (Fig. 3A). Isolated islets were cultured, and their transgene expression was evaluated. As shown in Fig. 3B and

D, Ad vector transduction *in vivo* succeeded in GFP expression in isolated islets. As had been expected, GFP was expressed even in the inside of islets, though not all islets effectively expressed GFP. We also observed that some islets express GFP throughout the islet. A typical image is shown in Fig. 3C. Furthermore, to determine whether β-cells were transduced, immunohistochemical analyses using an anti-insulin antibody were performed (Fig. 3E). Data showed that GFP expression was observed in insulin-producing cells, indicating that β-cells in the inside of islets were indeed transduced.

In vivo gene transfer to pancreatic islets using other routes, such as through the common bile duct [33,34] or a distal blood vessel from the pancreas [35], has been reported. However, the transgene was not expressed in islets efficiently and entirely and its expression pattern within the islet has not been analyzed in detail. This study should be valuable as a description of successful transduction into the inside of islets by the Ad vector.

In the present study, we have shown that pancreatic islets express CAR, a receptor for Ad, but that Ad vector-mediated transgene is expressed only in the periphery of the islets due to physical obstruction. We demonstrated that Ca^{2+}-free treatment before Ad vector transduction improves gene transduction into islets. Furthermore, Ad vector transduction through a proximal blood vessel *in vivo* and then cultivation of islets *in vitro* mediated efficient gene expression even in the inside of islets. Since pancreatic β-cells exist in the inner area of islets, this technique for Ad vector transductions could be very useful for basic research for β-cells and further therapeutic application for diabetes mellitus.

Acknowledgements

We are grateful to Dr. J. Miyazaki for generously providing the CA promoter and MIN6 cells. We also thank Drs. C. Yamada and K. Toyoda for their advice on anatomical techniques. This work was supported by grants for Health and Labour Sciences Research from the Ministry of Health, Labour, and Welfare of Japan.

References

[1] J.L. Gaglia, A.M. Shapiro, G.C. Weir, Islet transplantation: progress and challenge, Arch. Med. Res. 36 (2005) 273–280.
[2] J.R. Lakey, M. Mirbolooki, A.M. Shapiro, Current status of clinical islet cell transplantation, Methods Mol. Biol. 333 (2006) 47–104.
[3] S. Matsumoto, H. Noguchi, Y. Yonekawa, T. Okitsu, Y. Iwanaga, X. Liu, H. Nagata, N. Kobayashi, C. Ricordi, Pancreatic islet transplantation for treating diabetes, Expert Opin. Biol. Ther. 6 (2006) 23–37.
[4] L. Groop, Pathogenesis of type 2 diabetes: the relative contribution of insulin resistance and impaired insulin secretion, Int. J. Clin. Pract. Suppl. (2000) 3–13.
[5] A.J. Scheen, Pathophysiology of type 2 diabetes, Acta Clin. Belg. 58 (2003) 335–341.
[6] H. Basudev, P.M. Jones, S.L. Howell, Protein phosphorylation in the regulation of insulin secretion: the use of site-directed inhibitory peptides in electrically permeabilised islets of Langerhans, Acta Diabetol. 32 (1995) 32–37.
[7] P.Y. Benhamou, C. Moriscot, P. Prevost, E. Rolland, J. Chroboczek, S. Halimi, A methodology for an efficient and reproducible gene transfer into porcine islets using cationic liposomes, Transplant. Proc. 29 (1997) 2203.
[8] J.R. Lakey, A.T. Young, D. Pardue, S. Calvin, T.E. Albertson, L. Jacobson, T.J. Cavanagh, Nonviral transfection of intact pancreatic islets, Cell Transplant 10 (2001) 697–708.
[9] R.I. Mahato, J. Henry, A.S. Narang, O. Sabek, D. Fraga, M. Kotb, A.O. Gaber, Cationic lipid and polymer-based gene delivery to human pancreatic islets, Mol. Ther. 7 (2003) 89–100.
[10] C. Volpers, S. Kochanek, Adenoviral vectors for gene transfer and therapy, J. Gene Med. 6 (Suppl 1) (2004) S164–S171.
[11] H. Mizuguchi, T. Hayakawa, Targeted adenovirus vectors, Hum. Gene Ther. 15 (2004) 1034–1044.
[12] T.C. Becker, H. BeltrandelRio, R.J. Noel, J.H. Johnson, C.B. Newgard, Overexpression of hexokinase I in isolated islets of Langerhans via recombinant adenovirus. Enhancement of glucose metabolism and insulin secretion at basal but not stimulatory glucose levels, J. Biol. Chem. 269 (1994) 21234–21238.
[13] G. Leibowitz, G.M. Beattie, T. Kafri, V. Cirulli, A.D. Lopez, A. Hayek, F. Levine, Gene transfer to human pancreatic endocrine cells using viral vectors, Diabetes 48 (1999) 745–753.
[14] G. Bilbao, J.L. Contreras, I. Dmitriev, C.A. Smyth, S. Jenkins, D. Eckhoff, F. Thomas, J. Thomas, D.T. Curiel, Genetically modified adenovirus vector containing an RGD peptide in the HI loop of the fiber knob improves gene transfer to nonhuman primate isolated pancreatic islets, Am. J. Transplant. 2 (2002) 237–243.
[15] M. Narushima, T. Okitsu, A. Miki, C. Yong, K. Kobayashi, Y. Yonekawa, K. Tanaka, H. Ikeda, S. Matsumoto, N. Tanaka, N. Kobayashi, Adenovirus mediated gene transduction of primarily isolated mouse islets, ASAIO J. 50 (2004) 586–590.
[16] A.R. Barbu, G. Akusjarvi, N. Welsh, Adenoviral-mediated transduction of human pancreatic islets: importance of adenoviral genome for cell viability and association with a deficient antiviral response, Endocrinology 146 (2005) 2406–2414.
[17] H. Mizuguchi, M.A. Kay, Efficient construction of a recombinant adenovirus vector by an improved in vitro ligation method, Hum. Gene Ther. 9 (1998) 2577–2583.
[18] H. Mizuguchi, M.A. Kay, A simple method for constructing E1- and E1/E4-deleted recombinant adenoviral vectors, Hum. Gene Ther. 10 (1999) 2013–2017.
[19] H. Niwa, K. Yamamura, J. Miyazaki, Efficient selection for high-expression transfectants with a novel eukaryotic vector, Gene 108 (1991) 193–199.
[20] J.V. Maizel Jr., D.O. White, M.D. Scharff, The polypeptides of adenovirus. I. Evidence for multiple protein components in the virion and a comparison of types 2, 7A, and 12, Virology 36 (1968) 115–125.
[21] R. Sutton, M. Peters, P. McShane, D.W. Gray, P.J. Morris, Isolation of rat pancreatic islets by ductal injection of collagenase, Transplantation 42 (1986) 689–691.
[22] J.M. Bergelson, J.A. Cunningham, G. Droguett, E.A. Kurt-Jones, A. Krithivas, J.S. Hong, M.S. Horwitz, R.L. Crowell, R.W. Finberg, Isolation of a common receptor for Coxsackie B viruses and adenoviruses 2 and 5, Science 275 (1997) 1320–1323.
[23] T.J. Wickham, E. Tzeng, L.L. Shears II, P.W. Roelvink, Y. Li, G.M. Lee, D.E. Brough, A. Lizonova, I. Kovesdi, Increased in vitro and in vivo gene transfer by adenovirus vectors containing chimeric fiber proteins, J. Virol. 71 (1997) 8221–8229.
[24] I. Dmitriev, V. Krasnykh, C.R. Miller, M. Wang, E. Kashentseva, G. Mikheeva, N. Belousova, D.T. Curiel, An adenovirus vector with genetically modified fibers demonstrates expanded tropism via utilization of a coxsackievirus and adenovirus receptor-independent cell entry mechanism, J. Virol. 72 (1998) 9706–9713.
[25] V. Krasnykh, I. Dmitriev, G. Mikheeva, C.R. Miller, N. Belousova, D.T. Curiel, Characterization of an adenovirus vector containing a heterologous peptide epitope in the HI loop of the fiber knob, J. Virol. 72 (1998) 1844–1852.
[26] H. Mizuguchi, N. Koizumi, T. Hosono, N. Utoguchi, Y. Watanabe, M.A. Kay, T. Hayakawa, A simplified system for constructing recombinant adenoviral vectors containing heterologous peptides in the HI loop of their fiber knob, Gene Ther. 8 (2001) 730–735.
[27] N. Koizumi, H. Mizuguchi, N. Utoguchi, Y. Watanabe, T. Hayakawa, Generation of fiber-modified adenovirus vectors containing heterologous

peptides in both the HI loop and C terminus of the fiber knob, J. Gene Med. 5 (2003) 267–276.
[28] H. Mizuguchi, T. Sasaki, K. Kawabata, F. Sakurai, T. Hayakawa, Fiber-modified adenovirus vectors mediate efficient gene transfer into undifferentiated and adipogenic-differentiated human mesenchymal stem cells, Biochem. Biophys. Res. Commun. 332 (2005) 1101–1106.
[29] M. Ito, M. Kodama, M. Masuko, M. Yamaura, K. Fuse, Y. Uesugi, S. Hirono, Y. Okura, I. Kato, Y. Hotta, T. Honda, R. Kuwano, Y. Aizawa, Expression of coxsackievirus and adenovirus receptor in hearts of rats with experimental autoimmune myocarditis, Circ. Res. 86 (2000) 275–280.
[30] Z. Li, R.V. Sharma, D. Duan, R.L. Davisson, Adenovirus-mediated gene transfer to adult mouse cardiomyocytes is selectively influenced by culture medium, J. Gene Med. 5 (2003) 765–772.
[31] H. Wayland, Microcirculation in pancreatic function, Microsc. Res. Tech. 37 (1997) 418–433.
[32] L. Jansson, P.O. Carlsson, Graft vascular function after transplantation of pancreatic islets, Diabetologia 45 (2002) 749–763.
[33] S.E. Raper, R.P. DeMatteo, Adenovirus-mediated in vivo gene transfer and expression in normal rat pancreas, Pancreas 12 (1996) 401–410.
[34] H. Taniguchi, E. Yamato, F. Tashiro, H. Ikegami, T. Ogihara, J. Miyazaki, β-cell neogenesis induced by adenovirus-mediated gene delivery of transcription factor pdx-1 into mouse pancreas, Gene Ther. 10 (2003) 15–23.
[35] E. Ayuso, M. Chillon, J. Agudo, V. Haurigot, A. Bosch, A. Carretero, P.J. Otaegui, F. Bosch, In vivo gene transfer to pancreatic beta cells by systemic delivery of adenoviral vectors, Hum. Gene Ther. 15 (2004) 805–812.

Available online at www.sciencedirect.com
ScienceDirect
Biochemical and Biophysical Research Communications 353 (2007) 40–46
BBRC
www.elsevier.com/locate/ybbrc

Adult pancreatic islets require differential pax6 gene dosage

Akihiro Hamasaki [a], Yuichiro Yamada [a,b,*], Takeshi Kurose [a], Nobuhiro Ban [c], Kazuaki Nagashima [a], Akira Takahashi [a], Shimpei Fujimoto [a], Dai Shimono [a], Michio Fujiwara [d], Shinya Toyokuni [e], Yutaka Seino [a,f], Nobuya Inagaki [a,g]

[a] *Department of Diabetes and Clinical Nutrition, Kyoto University Graduate School of Medicine, Kyoto, Japan*
[b] *Department of Internal Medicine, Division of Endocrinology, Diabetes and Geriatric Medicine, Akita University School of Medicine, Akita, Japan*
[c] *Department of Physiology, Akita University School of Medicine, Akita, Japan*
[d] *Drug Safety Research Laboratories, Astellas Pharma Inc., Osaka, Japan*
[e] *Department of Pathology and Biology of Disease, Kyoto University Graduate School of Medicine, Kyoto, Japan*
[f] *Kansai Electric Power Hospital, Osaka, Japan*
[g] *CREST of Japan Science and Technology Cooperation (JST), Kyoto, Japan*

Received 15 November 2006
Available online 4 December 2006

Abstract

Pax6, a paired homeodomain transcription factor, plays crucial roles in morphogenesis of eye, central nervous system, and pancreatic islets. Recently, heterozygosity for pax6 mutation has been reported in some individuals with glucose intolerance and aniridia. To investigate the role of pax6 for pancreatic islet function, we examined the pancreatic phenotype of small eye rat strain (rSey^2) with a point mutation in the pax6 locus resulting in truncated PAX6 proteins. Analyses of the insulin secretory profile of heterozygous rSey^2/+ revealed that insulin secretion is significantly increased in response to membrane-depolarizing stimuli such as arginine, tolbutamide, and KCl. The processes of insulin granule exocytosis were suggested to be enhanced in rSey^2/+. On the other hand, pancreatic insulin and glucagon content and islet architecture in rSey^2/+ showed no significant differences compared to wild-type. These findings indicate differential requirements for pax6 gene dosage in displaying function and maintaining architecture of adult pancreatic islets.

Keywords: Pax6; Pancreatic islets; Insulin secretion; Arginine; Small eye; Pancreas

Transcription factors playing a role in pancreatic development have been shown to orchestrate the process of cell differentiation and transition by regulating the expression of numbers of genes [1,2]. To form the pancreas and organize pancreatic islets, multiple transcription factors play roles at precise steps in the developmental program. Various models in which these transcription factors are inactivated have revealed defects of pancreatic development or pancreatic islet morphogenesis.

The paired homeobox (Pax) family of transcription factors is involved in embryonic development of many organs including eyes, brain, kidney, thyroid gland, immune system, and the pancreas [3,4]. Two of its members, Pax4 and Pax6, play important roles in pancreatic endocrine cell differentiation [5,6]. In addition, Pax6 is essential for the development of eye and central nervous system and regulates the expression of various functional molecules in these tissues [7]. During the mouse embryogenesis, PAX6 protein can be detected already around E9.0 in the pancreatic endoderm, and its expression is maintained throughout pancreas development in all endocrine cells [8]. Analyses of pax6 mutant animals (Fig. 1) have revealed that differentiation of endocrine cells and the forming of proper islet architecture are severely affected in the fetal pancreas in the homozygous state. Pax6 knockout mice lack glucagon-producing α-cells and do not form proper islet structure [6]. In Sey^{NEU} mice, in which the PAX6 protein is

* Corresponding author.
E-mail address: yamada@gipc.akita-u.ac.jp (Y. Yamada).

0006-291X/$ - see front matter © 2006 Elsevier Inc. All rights reserved.
doi:10.1016/j.bbrc.2006.11.105

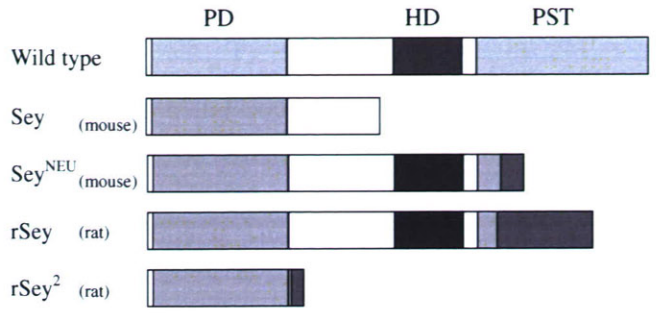

Fig. 1. Schematic diagram of coding region of pax6 gene and mutants. Wild-type PAX6 has a paired domain (PD), homeodomain (HD), and proline/serine/threonine rich transactivation domain (PST). Sey^{NEU} and rSey have a mutation, which results in a PAX6 protein that has a PD and HD but lacks the functional PST domain. Sey and $rSey^2$ (this study) have a mutation resulting in a PAX6 that has a PD but lacks the HD and PST domain completely.

truncated directly after the homeodomain, all four endocrine cell types are decreased in number [9]. Thus, Pax6 is involved in pancreatic development, particularly in endocrine cell differentiation and pancreatic islet organogenesis.

Transcription factors are involved not only in regulating pancreas development but also in pancreatic endocrine cell function. Many mutation models of transcription factors have shown that these mutations influence β-cell molecular events and the insulin secretory profile by altering the gene expression.

However, the role of PAX6 in adult islet function is little known except for the observations *in vitro* that PAX6 increases insulin, somatostatin, and glucagon gene transcription by binding with their promoters [9,10], and is involved in the regulation of enzymes and transcription factors [11,12]. The homozygous mice of pax6 knockout, Sey^{NEU} lack eyes and even model mice with conditional inactivation of pax6 in the endocrine pancreas [13] die shortly after birth, limiting the analyses of PAX6 function in the postnatal pancreatic islet function.

To investigate the mechanisms by which alterations in PAX6 affect islet function, we examined pancreatic islet function and architecture in small eye rat strain ($rSey^2$) with point mutation in the pax6 locus resulting in truncated PAX6 proteins [14] and found that in contrast to showing normal insulin secretion in response to glucose, $rSey^2/+$ showed surprisingly increased insulin release in response to membrane depolarizing stimuli and that $rSey^2/+$ had normal pancreatic islet architecture, indicating different requirement for pax6 gene dosage in the function and the morphology of the pancreatic islets.

Materials and methods

Animals. Mutant rats with small eyes ($rSey^2$) [14] were used in this study. Studies for the adult rats were performed in heterozygous ($rSey^2/+$) and their age-matched wild-type littermates. Homozygous rat embryos were obtained by inter-crossing male and female heterozygotes. Animal care and procedures were approved by the Animal Care Committee of Kyoto University.

Measurement of blood glucose, insulin, and glucagon levels. Blood glucose levels were measured by enzyme-electrode method. Plasma insulin levels were measured using ELISA kit (Shibayagi, Gunma, Japan). Plasma glucagon levels were measured using ELISA kit (Yanaihara Institute Inc., Shizuoka, Japan). Different groups of age-matched 20- to 24-week-old male rats were used for intraperitoneal glucose tolerance test. After an overnight fast, plasma insulin, glucagon, and glucose levels were measured and D-glucose (2 g/kg body weight) was loaded. In the insulin tolerance test, human insulin (1 U/kg) was injected subcutaneously in the fed condition. Blood samples were taken from the tail vein at indicated times.

Quantification of pancreatic peptide content. Protein was extracted from the dissected pancreas using acid extraction. Protein content was measured by Bio-Rad protein assay (Bio-Rad Laboratories, Hercules, CA). The amount of immunoreactive insulin was determined by RIA, using rat insulin as described [15]. The amount of immunoreactive glucagon was determined by using RIA kit (Linco Research, St. Charles, MO).

Immunohistochemistry. The pancreata of rats were removed under pentobarbital anesthesia (40 mg/kg body weight) and fixed in Bouin's solution. Pancreatic specimens were embedded in paraffin and sectioned at 3.5 μm. The avidin–biotin complex method with alkaline phosphatase or with peroxidase was used as previously described [16] with a slight modification. After deparaffinization, the following were sequentially applied: normal goat or rabbit serum (diluted to 1:75, Dako, Kyoto, Japan), primary antibodies, biotin-labeled goat anti-rabbit or rabbit anti-goat IgG serum (diluted to 1:300, Dako), and avidin–biotin–alkaline phosphatase complex or avidin–biotin–peroxidase complex (diluted to 1:100, Vector Laboratories, Burlingame, CA), followed by hematoxylin nuclear counterstaining. Staining was visualized in black and red by alkaline phosphatase substrate (Vector Laboratories) and in brown by peroxidase substrate. For PAX6 analysis, paraffin sections of pancreata were deparaffinized and autoclaved for 10 min at 121 °C in 10 mM citrate buffer (pH 6.0). The following primary antibodies were used: rabbit anti-insulin polyclonal antibody (diluted to 1:350, Dako), rabbit anti-glucagon serum (diluted to 1:500, OAL-123, Otsuka Assay Laboratory, Tokushima, Japan), rabbit anti-somatostatin polyclonal antibody (diluted to 1:200, Dako), rabbit anti-pancreatic polypeptide polyclonal antibody (diluted to 1:200, Dako), goat anti-GLUT2 polyclonal antibody (diluted to 1:50, C-19, Santa Cruz Biotechnology, Santa Cruz, CA) or rabbit anti-PAX6 polyclonal antibody (diluted to 1:20, H-295, Santa Cruz Biotechnology).

Isolated pancreatic perfusion. The pancreas was isolated as previously described [17]. All perfusions were accomplished with Krebs–Ringer Bicarbonate Buffer (KRBB) containing 0.25% bovine serum albumin (BSA, Fraction V, Sigma, St. Louis, MO) and 4.6% dextran (mean molecular weight 70,000; Pharmacia, Uppsala, Sweden). The perfusate was gassed with 95% O_2–5% CO_2 to maintain pH 7.4 at 37 °C. The flow rate was kept constant at 1.9 ml/min. After 20 min of equilibration, the perfusate was collected at 1-min intervals by cannula inserted into the portal vein. The collected effluent was frozen immediately with 1000 U aprotinin (Bayer, Leverkusen, German). The amount of immunoreactive insulin and immunoreactive glucagon was determined by RIA as described above.

Measurement of insulin release from isolated rat pancreatic islets. Isolated islets were cultured for 18 h in RPMI 1640 medium containing 10% fetal calf serum (FCS), 100 U/ml penicillin, and 100 μg/ml streptomycin. Insulin release from intact islets was monitored using batch incubation system described previously [18] with slight modifications. Cultured islets were preincubated at 37 °C for 30 min in KRBB supplemented with 2.8 mM glucose, 0.2% BSA, and 10 mM Hepes, adjusted to pH 7.4. Groups of 10 islets were then batch-incubated for 30 min in 0.4 ml of KRBB with test materials. The amount of immunoreactive insulin was determined by RIA as described above.

Measurement of intracellular Ca^{2+}. For intracellular Ca^{2+} ($[Ca^{2+}]_i$) measurement, cultured islets were loaded with fura-PE3 during 2 h of preincubation in the presence of 2 μM fura-PE3AM (Calbiochem, La Jolla, LA) as previously described [18]. Islets were placed at 36 ± 1 °C, superfused with KRBB containing 2.8 mM glucose and 10 mM Hepes adjusted to pH 7.4 for 30 min, and subsequently exposed to the medium containing a high concentration of K^+. The islets were excited successively

at 340 and 380 nm, and fluorescence emitted at 510 nm was captured by a charge-coupled device (CCD) camera (Micro Max 5-MHz System; Roper Industries, Trenton, NJ). Fluorescence signals at 340-nm (F340) and 380-nm (F380) were detected every 20 s. Results are expressed as the ratios (F340/F380).

Measurement of insulin release from electrically permeabilized islets. Cultured islets were preincubated with KRBB with 2.8 mM glucose and 0.2% BSA for 30 min. The islets were washed twice in cold potassium aspartate buffer (KA buffer) containing 140 mM KA, 7 mM $MgSO_4$, 2.5 mM EGTA, 30 mM Hepes (pH 7.0), and 0.5% BSA, with $CaCl_2$ added to a Ca^{2+} concentration of 30 nM. The islets were then permeabilized by high voltage discharge (four exposures, each of 450 μs duration, to an electrical field of 4.0 kV/cm) in KA buffer and washed once with the same buffer. Groups of electrically permeabilized islets were then batch-incubated for 30 min at 37 °C in 0.4 ml KA buffer with various concentrations of Ca^{2+} and ATP. At the end of the incubation period, permeabilized islets were pelleted by centrifugation (15000*g*, 180 s), and aliquots of the buffer were sampled. The amount of immunoreactive insulin was determined by RIA as described above.

Statistical analysis. Results are expressed as means ± SE. Statistical significance was evaluated by unpaired Student's *t*-test. $P < 0.05$ was considered significant.

Results and discussion

One intact allele in the pax6 gene is sufficient for maintenance of adult pancreatic islet architecture

In fetal pancreas in the homozygous state ($rSey^2/rSey^2$), insulin-positive cells are remarkably reduced and the alignment of the endocrine cells is not preserved (Fig. 2A). Especially, few or no glucagon-positive cells were found in the pancreas, and glucagon content could not be detected in RIA study of pancreas extract (data not shown). Recently, it has been reported that PAX6 is important especially for the endocrine cells to obtain final differentiation, rather than to proliferate [13]. Pax6 knockout mice have been shown to completely lack glucagon-producing cells in fetal pancreas [6]. In contrast, in the homozygous (Sey^{NEU}/Sey^{NEU}) mice, in which the PAX6 protein has a paired domain and homeodomain but lacks the transactivation domain (Fig. 1), the number of α-cells is reduced but is still present in the late fetal stage [9]. In the homozygous Sey mice [19] and $rSey^2$ rats (this study), in which the PAX6 protein has a paired domain but lacks a homeodomain and transactivation domain (Fig. 1), few or no glucagon-positive cells were detected in the later fetal stage in the homozygous state. These findings suggest that homeodomain is especially important in the formation of the pancreatic α-cells. In contrast to the homozygous fetal pancreatic islets, immunohistochemical evaluation of pancreata from adult heterozygote rats ($rSey^2/+$) revealed normal islet morphology with insulin-positive β-cells located in the center of the islet (Fig. 2B and C), and glucagon-positive α-cells (Fig. 2B and C), somatostatin-positive δ-cells (data not shown), and pancreatic polypeptide-positive PP-cells (data not shown) located in the periphery of the islets. Pancreatic insulin and glucagon contents in $rSey^2/+$ were the same as in wild-type (data not shown). Because of a recent report showing that expression of the glucose transporter GLUT2 was down-regulated in the pancreas of conditional inactivation of pax6 model mice [13], we examined GLUT2 expression in $rSey^2/+$ pancreatic islets. Adult $rSey^2/+$

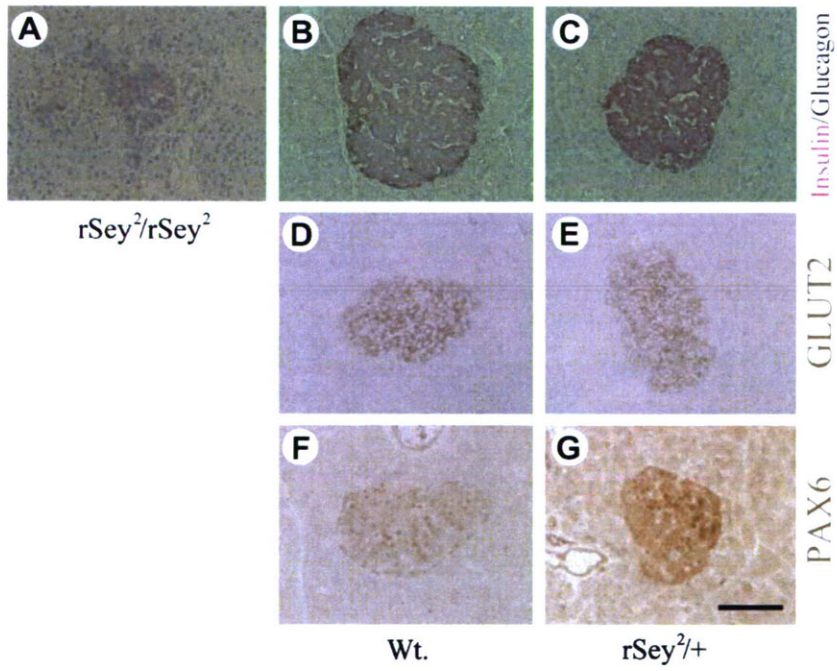

Fig. 2. One intact allele in the pax6 gene is sufficient for maintenance of adult pancreatic islet architecture. Immunohistochemical staining for islet protein was performed on paraffin-embedded sections of the pancreas. The sections were double-labeled for insulin (red) and glucagon (black) in the fetal (20.5E) homozygous state ($rSey^2/rSey^2$) (A) and adult wild-type (B), $rSey^2/+$ (C) rat pancreas or labeled for GLUT2 (D,E) and PAX6 (F,G) in the adult wild-type (D,F) and $rSey^2/+$ (E,G) rat pancreas. Bar 100 μm.

showed normal GLUT2 expression in the pancreatic endocrine cells (Fig. 2D and E). Thus, one allele of the wild-type pax6 gene is essential and sufficient to maintain morphologically normal pancreatic islets in adult. Anti-PAX6 antibody, which recognizes the C-terminus of PAX6 protein, was used to identify wild-type PAX6 protein derived from the wild-type pax6 allele, and rSey^2/+ was found to have similar PAX6 protein expression pattern in the nuclei of pancreatic islets (Fig. 2F and G).

Glucose-induced insulin secretion is preserved in heterozygous small eye rat strain (rSey^2/+)

Both male and female rSey^2/+ had similar body weight as wild-type rats (Fig. S1(A)). Pancreatic weight measured in males was similar in rSey^2/+ and wild-type (data not shown). Male rSey^2/+ showed normal fasting blood glucose levels, but had significantly higher fasting plasma insulin levels (Table 1). In the fed state, rSey^2/+ showed significantly lower blood glucose levels, and the plasma insulin level was similar in the two groups (Table 1). As these findings indicate relative hyperinsulinemia in rSey^2/+, we assessed the glucose-lowering effect of insulin by insulin tolerance test (ITT). rSey^2/+ and wild-type showed similar insulin sensitivity (Fig. S1(B)), indicating that the hyperinsulinemia is not derived from insulin resistance. In intraperitoneal glucose tolerance test (IPGTT), plasma glucose elevation elicited by glucose load in rSey^2/+ was similar to that of wild-type rats (Fig. S1(C)). Insulin secretion during IPGTT was also similar (Fig. S1(D)). Thus, it is possible that insulin secretion in response to secretagogues other than glucose is enhanced, resulting in hyperinsulinemia in rSey^2/+ rats. Glucagon is not a candidate as plasma glucagon levels were similar in the fasted and fed state (Table 1).

Insulin secretion induced by arginine is augmented in rSey^2/+ perfused pancreas

To determine which secretagogues contribute to the enhanced insulin release of rSey^2/+ in vivo, pancreatic perfusion was performed. rSey^2/+ rats showed the same biphasic insulin release from isolated perfused pancreas in response to stepwise increases in glucose concentration from 5.5 to 16.7 mM. However, insulin release in response to 10 mM arginine at the basal glucose level was significantly increased in rSey^2/+ rats (Fig. 3A). The integrated response to 10 mM arginine in the presence of 5.5 mM glucose was 1062 ± 285 ng of insulin in wild-type ($n = 5$) versus 2068 ± 131 ng of insulin in rSey^2/+ rats ($n = 5$) ($P < 0.05$) (Fig. 3B). On the other hand, rSey^2/+ rats showed similar glucagon release from the perfused pancreas in response to 10 mM arginine in the presence of 5.5 mM glucose (data not shown). This finding demonstrates that increased insulin response to 10 mM arginine in rSey^2/+ is not due to simultaneous enhancement of glucagon release.

Insulin secretory response to membrane-depolarizing stimuli in rSey^2/+ pancreatic islets

As one of the mechanisms by which arginine potentiates insulin release is direct depolarization of the pancreatic β-cell membrane, we examined insulin secretion evoked by membrane-depolarizing insulin secretagogues other than arginine. In batch incubation experiments, insulin release from isolated pancreatic islets in response to glucose stimulation was similar in rSey^2/+ (16.7 mM glucose: rSey^2/+ 0.82 ± 0.065 ng/islet/30 min ($n = 4$)) and wild-type rats (0.97 ± 0.087 ng/islet/30 min ($n = 4$)) ($P = 0.22$). However, insulin secretory responses to 10 mM arginine, 30 mM K^+, or 100 μM tolbutamide were significantly increased in rSey^2/+ pancreatic islets (10 mM arginine in the presence of 5.5 mM glucose: rSey^2/+ 0.55 ± 0.028 ng/islet/30 min ($n = 5$) vs. wild-type 0.21 ± 0.017 ng/islet/30 min ($n = 4$), $P < 0.001$; 30 mM K^+ in the presence of 2.8 mM glucose: rSey^2/+ 0.58 ± 0.035 ng/islet/30 min ($n = 5$) vs. wild-type 0.39 ± 0.040 ng/islet/30 min ($n = 4$), $P < 0.01$; 100 μM tolubutamide in the presence of 2.8 mM glucose: rSey^2/+ 0.45 ± 0.034 ng/islet/30 min ($n = 6$) vs. wild-type 0.31 ± 0.022 ng/islet/30 min ($n = 6$), $P < 0.01$) (Fig. 3C).

$[Ca^{2+}]_i$ elevation in pancreatic islets induced by 30 mM K^+-induced membrane depolarization in rSey^2/+ rats

To determine if the increase in K^+-induced insulin release in rSey^2/+ isolated islets is associated with increased intracellular Ca^{2+}, fura-PE3 was used to measure changes in $[Ca^{2+}]_i$. Five minutes before and 15 min after exposure to 30 mM K^+ in the presence of 2.8 mM glucose, $[Ca^{2+}]_i$ of rSey^2/+ islets was somewhat lower than that of wild-type islets (Fig. 4A and B). However, there was no difference between the depolarization-stimulated increment ratio in

Table 1
Blood glucose and plasma pancreatic hormone levels

	Blood glucose (mg/dl)		Plasma insulin (ng/ml)		Plasma glucagon (ng/ml)	
	Fed	Fasted	Fed	Fasted	Fed	Fasted
Wt	91 ± 2.1 ($n = 14$)	76 ± 1.0 ($n = 17$)	2.4 ± 0.36 ($n = 12$)	0.30 ± 0.09 ($n = 8$)	0.80 ± 0.03 ($n = 9$)	1.2 ± 0.44 ($n = 9$)
rSey^2/+	$80 \pm 1.8^{**}$ ($n = 11$)	72 ± 1.3 ($n = 15$)	1.9 ± 0.23 ($n = 11$)	$0.91 \pm 0.15^{*}$ ($n = 6$)	0.73 ± 0.05 ($n = 9$)	1.1 ± 0.22 ($n = 9$)

Values indicated as means ± SE.
* $P < 0.01$.
** $P < 0.001$ for rSey^2/+ vs. Wt.

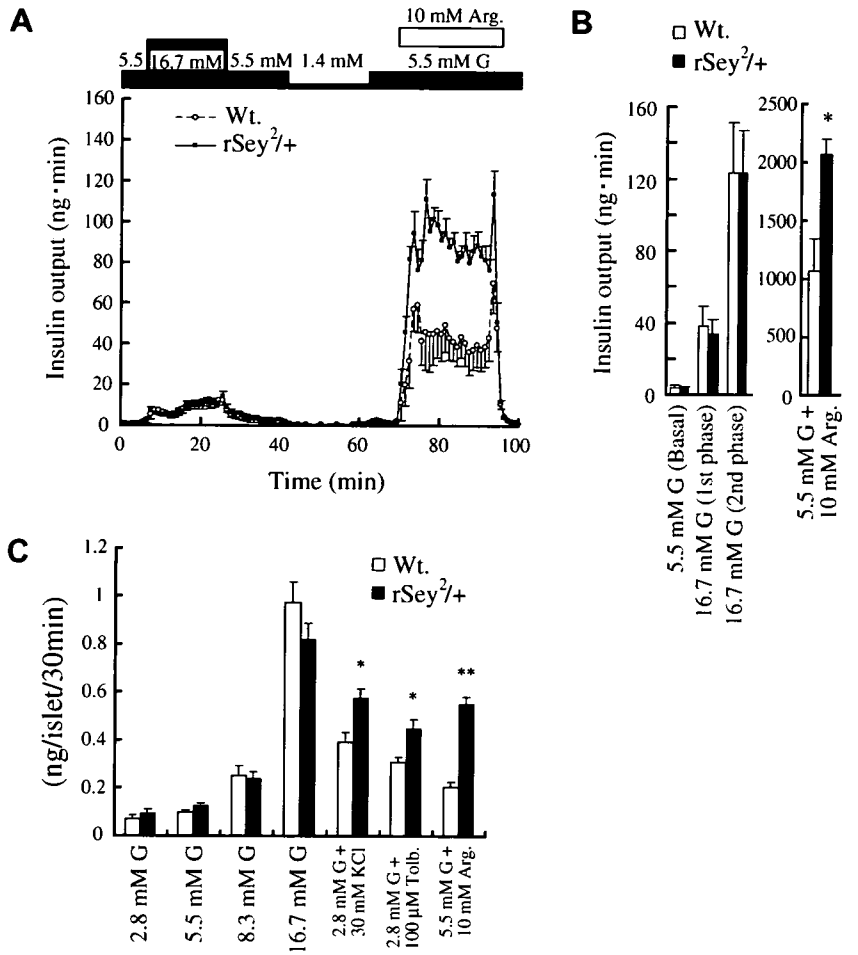

Fig. 3. (A,B) Insulin secretory responses from isolated perfused pancreas. Insulin release in response to glucose and arginine from the pancreas of rSey²/+ (■) and wild type littermates (○). Values are expressed as mean ± SE. (B) AUC of insulin release at 5.5 mM glucose (basal level, 1–6 min), first (6–13 min) and second (13–26 min) phase insulin release at 16.7 mM glucose, and insulin release in response to 5.5 mM glucose and 10 mM arginine (70–96 min) from the perfused pancreas of wild type (open bars, $n = 5$) and rSey²/+ (filled bars, $n = 5$). Values are expressed as mean ± SE. * $P < 0.05$, for rSey²/+ vs. wild type. G: glucose, Arg.: arginine. (C) Depolarization-induced insulin release from isolated islets. Insulin release from batch-incubated islets of wild type (open bars) and rSey²/+ (filled bars) was examined in response to the indicated concentrations of glucose with or without membrane depolarizing insulin secretagogues. Values are expressed as mean ± SE of 4–7 determinations from several experiments. * $P < 0.01$, ** $P < 0.001$ for rSey²/+ vs. wild type. G: glucose, Tolb.: tolbutamide, Arg.: arginine.

rSey²/+ islets and wild-type islets (rSey²/+ 1.076 ± 0.0033 vs. wild-type 1.073 ± 0.0044, $P = 0.54$) (Fig. 4B).

Ca^{2+} efficacy in insulin release under low ATP condition in rSey²/+ pancreatic islets

To determine if intracellular Ca^{2+} efficacy is altered in rSey²/+ islets, we measured insulin release from pancreatic β-cell at $[Ca^{2+}]_i$ clamped by extracellular medium. As shown in Fig. 4C and D, raising the Ca^{2+} concentration from 30 nM to 10 μM elicited an increase in insulin release from electrically permeabilized islets. In the presence of 5 mM ATP, insulin release in rSey²/+ was similar to wild-type at all Ca^{2+} concentrations (Fig. 4C). This result is commensurate with the findings that rSey²/+ has a similar insulin secretory response to glucose as wild-type. However, in the presence of 1 mM ATP, insulin release in rSey²/+ islets at Ca^{2+} concentrations from 30 to 1000 nM was greater than in wild-type islets (at 30 nM Ca^{2+}: rSey²/+ 0.44 ± 0.031 vs. wild-type 0.30 ± 0.032 ($n = 8$), $P < 0.01$; at 100 nM Ca^{2+}: rSey²/+ 0.44 ± 0.039 vs. wild-type 0.32 ± 0.035 ($n = 8$), $P < 0.05$; at 300 nM Ca^{2+}: rSey²/+ 0.66 ± 0.040 vs. wild-type 0.45 ± 0.052 ($n = 7$), $P < 0.01$; at 1000 nM Ca^{2+}: rSey²/+ 0.85 ± 0.033 vs. wild-type 0.54 ± 0.074 ng/islet/30 min ($n = 8$), $P < 0.01$) (Fig. 4D). This might well underlie the increased insulin secretion seen in rSey²/+ β-cells in response to membrane depolarizing stimuli at the basal glucose level.

Thus, our findings show that pax6 gene mutation modifies the insulin secretory profile of adult pancreatic islets and that the disturbance in the insulin secretory mechanism in rSey²/+ pancreatic islets is in the triggering of insulin granule exocytosis by the rise in $[Ca^{2+}]_i$, although the molecular mechanism remains to be determined.

In this study, rSey²/+ islets showed increased insulin response to membrane-depolarizing stimuli such as

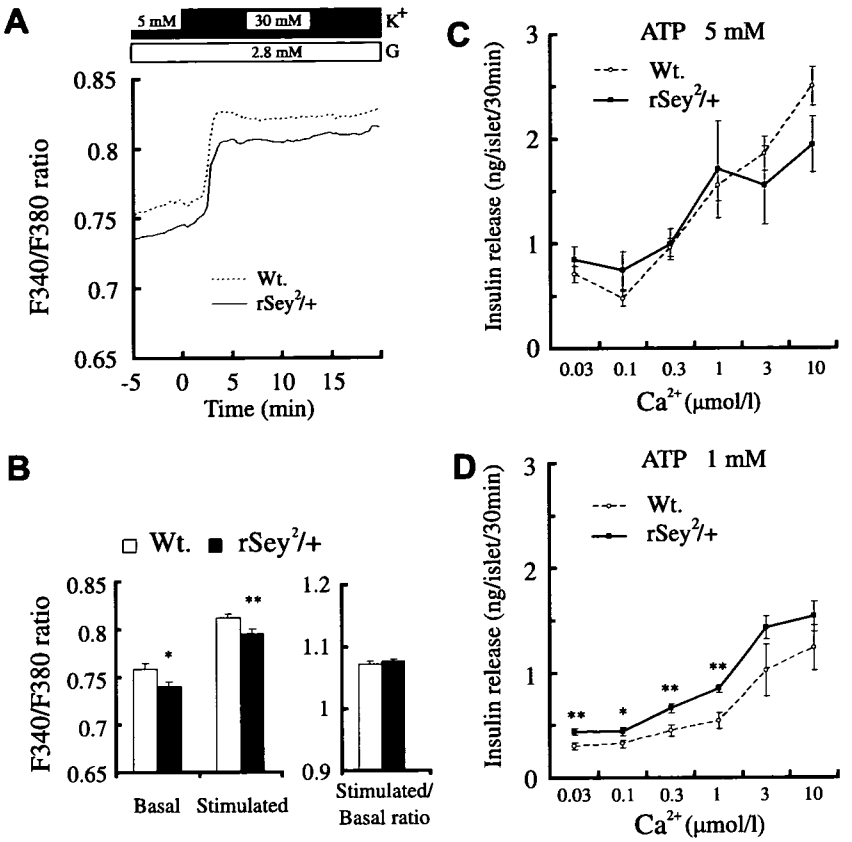

Fig. 4. (A,B) Fluorescence measurement of $[Ca^{2+}]_i$ elevation induced by 30 mM K^+-induced depolarization in the presence of 2.8 mM glucose. (A) Time course of $[Ca^{2+}]_i$ in perfused islets. Values represent mean of 83 (wild-type) and 74 (rSey^2/+) determinations from the several experiments. (B) Left, average values calculated from the data from (A). Basal, average values from −5 to 0 min in the presence of 5 mM K^+ with 2.8 mM glucose. Stimulated, average value from 0 to 15 min in the presence of 30 mM K^+ with 2.8 mM glucose. Right, values represent means ± SE of the ratio of stimulated value to basal value. $*P < 0.05$, $**P < 0.01$ for rSey^2/+ vs. wild-type. G, glucose. (C,D) Ca^{2+} dose–response of insulin release from electrically permeabilized islets. After preincubation with 2.8 mM glucose for 50 min, islets were electrically permeabilized and incubated with medium containing Ca^{2+} and ATP at the concentration indicated in the figure. Ca^{2+} dose-dependent insulin release from electrically permeabilized islets of wild-type (○) and rSey^2/+ (■) in the presence of 5 mM (C) or 1 mM (D) ATP. Values represent means ± SE of 7–8 determinations in the same experiment for each. $*P < 0.05$, $**P < 0.01$ for rSey^2/+ vs. wild-type.

arginine. This findings may underlie the relative hyperinsulinemia of rSey^2/+ rats in vivo. In contrast to rSey^2/+, it recently has been reported that rSey/+, another small eye rat strain (Fig. 1), in which the pax6 mutation is located in the transactivation domain [20], has impaired insulin response to glucose but show normal insulin secretory response to arginine [21]. These differences in pancreatic islet function suggest that pax6 plays a key role in regulating the insulin secretory response to various nutrients in pancreatic islets.

Morphological and functional analyses of rSey^2/+ pancreatic islets have important implications regarding gene dosage on pancreatic islet architecture and function. The maintenance of islet morphology in adult pancreas showed low sensitivity to quantity of pax6 gene. In contrast, islet function is necessarily more sensitive to alterations in pax6 gene. While the pax6 gene mutation in rSey^2/+ altered the insulin secretory profile, glucagon secretion was unaffected by the same mutation. These findings indicate that for displaying normal function, insulin-secreting β-cells among the pancreatic islet hormone-secreting cells require higher quantity of pax6 gene than glucagon-secreting α-cells. Outside of the pancreas, it is well known that pax6 is a key regulator of eye formation and that heterozygous pax6 mutations result in eye size reduction due to sensitivity to pax6 gene dosage for eye formation [22,23]. rSey^2/+ eye size also is reduced [14], indicating that the pancreas and the eye of same individual has differing sensitivity to the quantity of pax6 gene. Thus, there are differential dosage requirements for the pax6 gene between organs as well as between morphological and functional characteristics.

Acknowledgments

This study was supported in part by Grants-in-Aid for Scientific Research from the Ministry of Education, Culture, Sports, Science and Technology, Japan, by Health and Labour Sciences Research Grants for Comprehensive Research on Aging and Health, Labor and Welfare, Japan, and by the 21st Century Center of Excellence Program, Japan.

Appendix A. Supplementary data

Supplementary data associated with this article can be found, in the online version, at doi:10.1016/j.bbrc.2006.11.105.

References

[1] H. Edlund, Pancreatic organogenesis—developmental mechanisms and implications for therapy, Nat. Rev. Genet. 3 (2002) 524–532.
[2] M.E. Wilson, D. Scheel, M.S. German, Gene expression cascades in pancreatic development, Mech. Dev. 120 (2003) 65–80.
[3] A. Mansouri, M. Hallonet, P. Gruss, Pax genes and their roles in cell differentiation and development, Curr. Opin. Cell Biol. 8 (1996) 851–857.
[4] E. Dahl, H. Koseki, R. Balling, Pax genes and organogenesis, Bioessays 19 (1997) 755–765.
[5] B. Sosa-Pineda, K. Chowdhury, M. Torres, G. Oliver, P. Gruss, The Pax4 gene is essential for differentiation of insulin-producing beta cells in the mammalian pancreas, Nature 386 (1997) 399–402.
[6] L. St-Onge, B. Sosa-Pineda, K. Chowdhury, A. Mansouri, P. Gruss, Pax6 is required for differentiation of glucagon-producing alpha-cells in mouse pancreas, Nature 387 (1997) 406–409.
[7] T.I. Simpson, D.J. Price, Pax6; a pleiotropic player in development, Bioessays 24 (2002) 1041–1051.
[8] C. Dohrmann, P. Gruss, L. Lemaire, Pax genes and the differentiation of hormone-producing endocrine cells in the pancreas, Mech. Dev. 92 (2000) 47–54.
[9] M. Sander, A. Neubuser, J. Kalamaras, H.C. Ee, G.R. Martin, M.S. German, Genetic analysis reveals that PAX6 is required for normal transcription of pancreatic hormone genes and islet development, Genes Dev. 11 (1997) 1662–1673.
[10] F.G. Andersen, J. Jensen, R.S. Heller, H.V. Petersen, L.I. Larsson, O.D. Madsen, P. Serup, Pax6 and Pdx1 form a functional complex on the rat somatostatin gene upstream enhancer, FEBS Lett. 445 (1999) 315–320.
[11] C.C. Martin, J.K. Oeser, R.M. O'Brien, Differential regulation of islet-specific glucose-6-phosphatase catalytic subunit-related protein gene transcription by Pax-6 and Pdx-1, J. Biol. Chem. 279 (2004) 34277–34289.
[12] S.E. Samaras, M.A. Cissell, K. Gerrish, C.V. Wright, M. Gannon, R. Stein, Conserved sequences in a tissue-specific regulatory region of the pdx-1 gene mediate transcription in Pancreatic beta cells: role for hepatocyte nuclear factor 3β and Pax6, Mol. Cell. Biol. 22 (2002) 4702–4713.
[13] R. Ashery-Padan, X. Zhou, T. Marquardt, P. Herrera, L. Toube, A. Berry, P. Gruss, Conditional inactivation of Pax6 in the pancreas causes early onset of diabetes, Dev. Biol. 269 (2004) 479–488.
[14] N. Osumi, A. Hirota, H. Ohuchi, M. Nakafuku, T. Iimura, S. Kuratani, M. Fujiwara, S. Noji, K. Eto, Pax-6 is involved in the specification of hindbrain motor neuron subtype, Development 124 (1997) 2961–2972.
[15] K. Tsuji, T. Taminato, M. Usami, H. Ishida, N. Kitano, H. Fukumoto, G. Koh, T. Kurose, Y. Yamada, H. Yano, Y. Seino, H. Imura, Characteristic features of insulin secretion in the streptozotocin-induced NIDDM rat model, Metabolism 37 (1988) 1040–1044.
[16] Y. Ihara, S. Toyokuni, K. Uchida, H. Odaka, T. Tanaka, H. Ikeda, H. Hiai, Y. Seino, Y. Yamada, Hyperglycemia causes oxidative stress in pancreatic β-cells of GK rats, a model of type 2 diabetes, Diabetes 48 (1999) 927–932.
[17] T. Kurose, Y. Seino, S. Nishi, K. Tsuji, T. Taminato, K. Tsuda, H. Imura, Mechanism of sympathetic neural regulation of insulin, somatostatin, and glucagon secretion, Am. J. Physiol. 258 (1990) E220–E227.
[18] S. Fujimoto, E. Mukai, Y. Hamamoto, T. Takeda, M. Takehiro, Y. Yamada, Y. Seino, Prior exposure to high glucose augments depolarization-induced insulin release by mitigating the decline of ATP level in rat islets, Endocrinology 143 (2002) 213–221.
[19] R.S. Heller, D.A. Stoffers, A. Liu, A. Schedl, E.B. Crenshaw 3rd, O.D. Madsen, P. Serup, The role of Brn4/Pou3f4 and Pax6 in forming the pancreatic glucagon cell identity, Dev. Biol. 268 (2004) 123–134.
[20] T. Matsuo, N. Osumi-Yamashita, S. Noji, H. Ohuchi, E. Koyama, F. Myokai, N. Matsuo, S. Taniguchi, H. Doi, S. Iseki, et al., A mutation in the Pax-6 gene in rat small eye is associated with impaired migration of midbrain crest cells, Nat. Genet. 3 (1993) 299–304.
[21] A. Kuroda, H. Kaneto, Y. Fujitani, H. Watada, Y. Nakatani, Y. Kajimoto, M. Matsuhisa, Y. Yamasakai, M. Fujiwara, Mutation of the Pax6 gene causes impaired glucose-stimulated insulin secretion, Diabetologia 47 (2004) 2039–2041.
[22] A. Schedl, A. Ross, M. Lee, D. Engelkamp, P. Rashbass, V. van Heyningen, N.D. Hastie, Influence of PAX6 gene dosage on development: overexpression causes severe eye abnormalities, Cell 86 (1996) 71–82.
[23] C.D. van Raamsdonk, S.M. Tilghman, Dosage requirement and allelic expression of PAX6 during lens placode formation, Development 127 (2000) 5439–5448.

European Journal of Neuroscience, Vol. 25, pp. 2349–2363, 2007 doi:10.1111/j.1460-9568.2007.05499.x

Disruption of Kir6.2-containing ATP-sensitive potassium channels impairs maintenance of hypoxic gasping in mice

Akari Miyake,[1,*] Katsuya Yamada,[1,2,5,*] Tomohiro Kosaka,[1] Takashi Miki,[3] Susumu Seino[3] and Nobuya Inagaki[1,4,5]
[1]Department of Physiology, Akita University School of Medicine, Akita, Japan
[2]Department of Physiology, Hirosaki University School of Medicine, Aomori, Japan
[3]Division of Cellular and Molecular Medicine, Kobe University Graduate School of Medicine, Kobe, Japan
[4]Department of Diabetes and Clinical Nutrition, Kyoto University Graduate School of Medicine, 54 Kawahara-cho, Shogoin, Sakyo-ku, Kyoto 606-8577, Japan
[5]CREST of Japan Science and Technology Agency, Kawaguchi, Saitama, Japan

Keywords: depression, hypoxia, ATP-sensitive potassium channel, sigh, tachypnea

Abstract

Hypoxic gasping emerges under severe hypoxia/ischemia in various species, exerting a life-protective role by assuring minimum ventilation even in loss of consciousness. However, the molecular basis of its generation and maintenance is not well understood. Here we found that mice lacking Kir6.2- but not Kir6.1-containing ATP-sensitive potassium (K_{ATP}) channels [knockout (KO) mice] exhibited few gasps when subjected to abrupt ischemia by decapitation, whereas wild-type mice all exhibited more than 10 gasps. Under anesthesia, wild-type mice initially responded to severe hypoxic insult with augmented breathing (tachypnea) accompanied by sighs and subsequent depression of respiratory frequency. Gasping then emerged and persisted stably (persistent gasping); if the hypoxia continued, several gasps with distinct patterns appeared (terminal gasping) before cessation of breathing. KO mice showed similar hypoxic responses but both depression and the two types of gasping were of much shorter duration than in wild-type mice. Moreover, in the unanesthetized condition, the onset of terminal gasping in KO mice, which was always earlier than in wild-type mice, was unaltered by decreasing O_2 concentrations within the severe range (4.5–7.0%), whereas onset in wild-type mice became earlier in response to lowered O_2 concentrations. Thus, the mechanism responsible for regulating the hypoxic response in accordance with the severity of the hypoxia was dysfunctional in these KO mice, suggesting that Kir6.2-containing K_{ATP} channels are critically involved in the maintenance rather than the generation of hypoxic gasping and depression of respiratory frequency.

Introduction

Under severe hypoxia/ischemia, as in stroke and cardiac/pulmonary failure, reduced O_2 supply to the brain triggers a sequence of respiratory responses including an initial augmentation (tachypnea) followed by a depression of respiratory frequency and, if prolonged, electroencephalogram silence marking hypoxic coma. In this state, gasping, a spontaneous respiratory activity, can emerge and thereby improve the blood oxygenation state and increase the recovery rate (St. John & Knuth, 1981; Sanocka *et al.*, 1992; Khurana & Thach, 1996; Fewell, 2005). Despite its critical importance in protection of life, the molecular basis underlying such gasping remains poorly understood.

ATP-sensitive potassium (K_{ATP}) channels (Noma, 1983) consisting of pore-forming Kir6.*x* and sulfonylurea receptor (SUR) subunits (Inagaki *et al.*, 1995, 1996) couple the intracellular metabolic state of cells to electrical activity at the plasma membrane (Ashcroft, 1988; Seino, 1999). K_{ATP} channels are expressed in brain in various nuclei including brainstem (Mourre *et al.*, 1989; Mironov *et al.*, 1998) but their physiological role is only partially clear. We previously reported that mice lacking the Kir6.2 subunit of K_{ATP} channels [knockout (KO) mice] (Miki *et al.*, 1998) are extremely susceptible to generalized seizure after brief hypoxia (Yamada *et al.*, 2001). When subjected to severe hypoxia (~5% O_2), KO mice soon exhibited very low-voltage electroencephalogram, indicating loss of consciousness. Tonic convulsion then lasted for several seconds, after which generalized seizure was observed in the electroencephalogram, whereas in wild-type mice, medium to low-voltage waves predominated and gasping emerged after prolonged hypoxia. During the course of the study, we found that KO mice exhibited fewer gasps under hypoxia (unpublished observation), indicating involvement of the K_{ATP} channels in control of gasping.

Extensive studies on gasping have been reported (St. John & Knuth, 1981; Selle & Witten, 1941; Holowach-Thurston *et al.*, 1974; Khurana & Thach, 1996; Wang *et al.*, 1996; Ramirez *et al.*, 1998; Lieske *et al.*, 2000; Paton *et al.*, 2006). However, very different methods of inducing hypoxia have been used *in vivo* and *in vitro*, and characterizing gasping by the various methodologies is problematic (Ramirez & Lieske, 2003).

In the present study, we used three protocols to investigate the regulatory mechanism of hypoxic gasping in mice, including abrupt ischemia by decapitation and hypoxia in anesthetized and unanesthetized conditions. Differences in hypoxic responses between wild-type

Correspondence: Dr Nobuya Inagaki, [4]Department of Diabetes and Clinical Nutrition, as above.
E-mail: inagaki@metab.kuhp.kyoto-u.ac.jp

*A.M. and K.Y. contributed equally to this work.

Received 11 December 2006, revised 19 February 2007, accepted 22 February 2007

and Kir6.2 KO mice were investigated using methods including monitoring expiratory flow with a thermistor airflow sensor, respiratory body movement with a piezoelectric transducer (PZT) device (Sato *et al.*, 2006), expired O_2/CO_2 with a gas analyser and activity of the phrenic nerve. An experiment in unanesthetized condition was required because respiration under severe hypoxia is affected by both anesthesia level and body temperature (Fazekas *et al.*, 1941; Miller, 1949; Secher & Wilhjelm, 1968; Fewell, 2005), and could not be equalized among anesthetized mice subjected to phrenic nerve recordings. Mice exhibiting gasping were considered to be in a condition of hypoxic coma (loss of consciousness) based on electroencephalogram (Yamada *et al.*, 2001).

Materials and methods

Animals

Fifty-nine wild-type mice (C57BL/6J), 52 mice lacking Kir6.2-containing K_{ATP} channels (Miki *et al.*, 1998) and four Kir6.1-deficient mice (Miki *et al.*, 2002) were used in accordance with a protocol approved by the Akita University Institutional Committee for Animal Studies and followed the Akita University Guidelines for Animal Experimentation. The Kir6.2 and Kir6.1 genes were cloned from a 129/Sv mouse genomic DNA library. The mutant mice were backcrossed more than four times to C57BL/6 mice. All mice were adult males (>2 months). Urethane anesthesia (1.4 g/kg, i.p.) was used in all experiments under anesthetic condition. The anesthesia level was evaluated by monitoring respiration frequency and electrocardiogram. For the brief hypoxia experiment (see Results), the heart rate (652.6 ± 4.5/min, $n = 23$) and respiratory frequency before hypoxic challenge (4.0 ± 0.1 Hz, $n = 23$) of wild-type mice were not significantly different from those of KO mice (643.7 ± 7.1/min and 3.8 ± 0.1 Hz, respectively. $n = 12$). For the prolonged hypoxia experiment, the heart rate (628.7 ± 3.8/min, $n = 4$) and respiratory frequency before hypoxic challenge (4.0 ± 0.1 Hz, $n = 4$) of wild-type mice were not significantly different from those of KO mice (613.2 ± 14.8/min and 4.2 ± 0.2 Hz, respectively. $n = 5$).

Abrupt ischemia caused by decapitation

To compare central regulation of gasping of wild-type and KO mice in abrupt ischemia, the whole head was isolated by decapitation while the mouse was restrained on a PZT device, which converts mechanical motion into an electrical signal (PCT/JP03/01109; Sato *et al.*, 2006). The buffered PZT-produced signals were amplified by a custom-made amplifier (×1 or ×10), digitalized and filtered offline by commercially available software (CLAMPEX 8 and CLAMPFIT 8, Molecular Devices, Sunnyvale, CA, USA). To distinguish gasping from other body movements, respiration was simultaneously monitored by four infrared CCD cameras from different directions and stored on video tape or DVD. The number of gasps was counted from the stored image in reference to sharp deflections in the PZT-derived vibration signal. Gasps comprising double openings of the jaw (double or diphasic gasps) (Selle, 1944) were counted as two gasps in these experiments.

After dissection, brains were removed and fixed in 4% paraformaldehyde at 4 °C for later examination of the dissected portion of the spinal cord. Only cases of dissection caudal to the C2 level were analysed in the present study, as no gasp was seen when the dissection was made at the C0–C1 level in both wild-type and KO mice. Although we did not investigate this matter in the present study, it is possible that impairment of the C1 cell group has some role in the central regulation of respiration (Gang *et al.*, 1995).

Hypoxia experiments under anesthesia

Tracheotomy was performed in urethane-anesthetized mice. One end of a bent stainless steel cannula (6-mm-long, 18G flat-end needle) was inserted into the trachea and the open end was connected to a 2.5-mL open syringe (Fig. 1A). Care was taken to minimize the dead volume in the tracheal cannula and the tube connecting the cannula to the syringe. From the open end of the syringe, two Pharmed tubes (Saint-Gobain Performance Plastics, OH, USA) were inserted and fixed firmly to the syringe with a glue; one (thicker, internal diameter 2 mm) was for introducing hypoxic gas or air into the syringe and the other (thinner, internal diameter 1 mm) was set closer to the cannula end for effective sampling of the expired gas. The gas expired from the cannula, which was diluted to a certain extent by the atmosphere in the syringe, was continuously sampled (10 mL/min) and measured by an O_2/CO_2 analyser (1H-26, GE Healthcare, Tokyo, Japan).

In the syringe, changes in the temperature of outflow from the tracheal cannula were simultaneously monitored by a conventional thermistor-type airflow sensor (type 45257, GE Healthcare). To detect respiratory body movement, a PZT sensor, which was integrated into a heater plate for maintaining body temperature, was used (Sato *et al.*, 2006). As gasping is strongly affected by temperature (Fazekas *et al.*, 1941; Miller, 1949; Fewell, 2005), special care was taken to keep the rectal temperature under anesthesia at 37.0 ± 0.1 °C using a custom-made heater device, while also monitoring the surface temperature of the heater (Japanese Patent no. 3685983; Sato *et al.*, 2006). The rectal temperature was recorded with a thin thermistor probe 2 cm from the anus. Electrocardiogram was measured between the right forepaw and left hindpaw.

Two types of hypoxia experiments under anesthesia for either 60 s or a more prolonged period until cessation were conducted. Hypoxia was produced by switching the gas introduced into the syringe from room air to pre-mixed hypoxic gas with the same flow rate (500 mL/min) using microprocessor-controlled, electromagnetic three-way valves. The pre-mixed gas was produced from O_2 and N_2 gas by using mass flow meters (SEC-E40, HORIBA STEC, Kyoto,

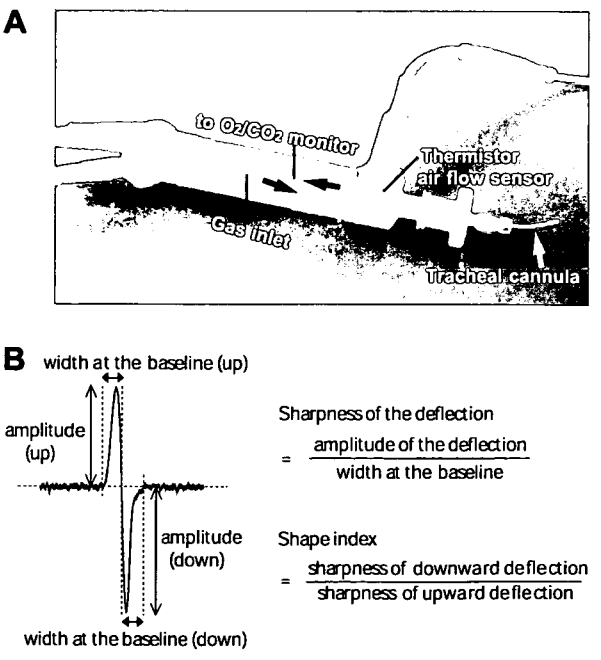

FIG. 1. Apparatus for introducing hypoxia to spontaneously breathing mouse in anesthetized condition (A) and piezoelectric transducer shape index (B).

Japan). When pre-mixed gas of 4.5–5.0% O_2 was introduced, the O_2 concentration within the syringe at 60 s after the opening of the valves was 5.0–5.5% (~16 s were needed for the atmosphere in the syringe to reach 5.5% O_2 for a pre-mixed value of 4.5% O_2). Thus, in the 60-s brief hypoxia experiment, the O_2 concentration was expressed as the value at 60 s after valve opening. In the prolonged hypoxia experiment, although the O_2 concentration reached closer to the pre-mixed value, the concentration at 60 s after the valve opening was also used to indicate the value.

In all of the prolonged hypoxia experiments and in some of the 60-s brief hypoxia experiments, the right phrenic nerve was identified and unsheathed. Nerve activity was recorded with bipolar silver electrodes (diameter 0.1 mm, interpolar distance unfixed), amplified (time constant 0.3 ms, cut-off frequency of low-pass filter 1 kHz; Bioelectric Amplifier 4124, GE Healthcare) and stored in a PC (see Digitalization section below).

Tachypnea, sigh and depression frequency in anesthetized condition

The onset of tachypnea was marked as the time point at which the ratio of the respiratory frequency under hypoxia relative to the mean frequency before hypoxia (0–10 s) continuously exceeded 100%, except for a possible single fluctuation.

Sigh was characterized by a large inspiration followed by an extraordinarily large-amplitude expiration and a brief post-sigh apneic period (Nakamura *et al.*, 2003). The magnitude of the expiration could be detected by a large upward deflection in the traces of expired CO_2 as well as by the thermistor airflow sensor. The upward deflection in the thermistor trace was followed by a wide and deep downward deflection, which was clearly distinguished from those of neighboring large breaths in the brief hypoxia experiment (see Results). The shape of the downward deflection of sigh reflects both the amplitude and width of the preceding upward deflection, the amplitude of the downward deflection becoming larger as the width of the upward deflection becomes wider according to the time constant of an AC amplifier (0.3 s) and software high-pass filter (> 1 Hz). In addition, the presence of the post-sigh apneic period also affected the shape of the downward deflection. A similar consideration is also applicable in discrimination of terminal gasping and persistent gasping in the prolonged hypoxia experiment (see Results).

The onset of depression was defined as the time point at which the ratio of the respiratory frequency under hypoxia relative to the mean frequency before hypoxia fell below 100%. The duration of depression was counted as the period from its onset to the beginning of persistent gasping (see next paragraph).

Shape index of piezoelectric transducer response under anesthesia

In the anesthetized condition, both inspiratory and expiratory body movement can be detected directly as vertical motion by the PZT device placed under the body (Sato *et al.*, 2006). The PZT device was moveable, and was set in the position at which the upward and downward deflections of the PZT signal corresponded to inspiratory and expiratory body movement, respectively, which was confirmed by simultaneously monitored changes in the phrenic nerve discharge, expiratory CO_2 and airflow in the outlet of the tracheal cannula. Under urethane anesthesia, respiratory body movement detected by PZT showed a biphasic shape. Evaluation of the symmetry of the upward and downward deflections in PZT shape was accomplished as follows (Fig. 1B). To measure the sharpness of the deflection, the amplitude was divided by its width at the baseline. The ratio of the sharpness of the downward deflection to the sharpness of the upward deflection is the shape index, which is 1 when the shapes of the upward and downward deflections are symmetrical.

Hypoxia under unanesthetized condition

Individual mice were subjected to hypoxia while held in a conical skirted, tapered centrifuge tube (internal diameter 25–27 mm, no. 62.559, Sarstedt, Numbrecht, Germany) with mouth and nose protruding slightly from the opening (diameter 4.5 mm) in the bottom of the tube for breathing gas introduced from the inlet (Fig. 2). The dead volume outside the hole was minimized with silicon filling. The dead volume within the tube was decreased by a soft rubber inner plug, the position of which was adjusted to minimize disturbances of natural respiration. Expired gas from the centrifuge tube was monitored by an O_2/CO_2 analyser. A very slow flow rate (75 mL/min) for introducing pre-mixed gas (O_2 ranging from 4.5 to 7.0% or air for control) was selected to detect gasping while minimizing seizure. At this flow rate, individual expiratory breaths during gasping could be detected by sharp deflections in the sampled CO_2 trace. When the mouse breathed room air, the O_2 concentration in the sampled expired gas was slightly lower and the CO_2 concentration was higher due to the slow flow rate.

The whole centrifuge tube was placed on the PZT device. The respiratory body movement of the mouse caused a small vibration of the rubber plug (Fig. 2) and a drift of the center of gravity of the centrifuge tube. The resulting angular moment of the tube was transferred to the PZT device as vertical motion. Inspiratory body movement produced downward deflections of the PZT signal in the resting eupneic condition. Thus, the respiratory frequency in the unanesthetized condition could be measured by PZT deflections while being confirmed by percentage CO_2 changes except when large body movements overlapped.

The onset of tachypnea in unanesthetized condition was determined as the time point at which the extrapolated rising phase of the relative respiratory frequency in tachypnea intersected the 100% line (mean respiratory frequency before hypoxic challenge) (see Fig. 11A2 and B2). The onset of depression subsequent to tachypnea was similarly determined but by using the falling phase in tachypnea. The onset of terminal gasping was determined as the time point at which the duration between positive and negative PZT deflections abruptly became wide during the period before cessation. Precise determination of the duration of terminal gasping in unanesthetized condition was difficult because the convulsive movements just before cessation also produced deflections in the PZT signal and an increase in CO_2.

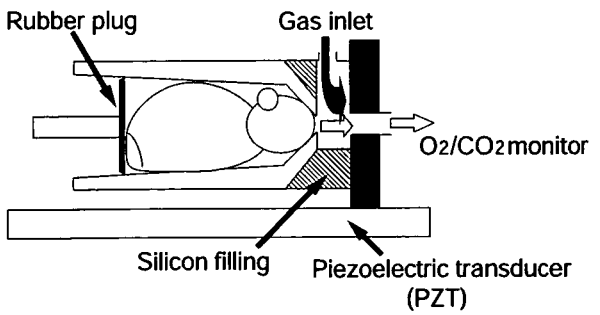

FIG. 2. Apparatus for introducing hypoxia to mouse in unanesthetized condition. PZT, piezoelectric transducer.

Digitalization

All bioelectric signals, including PZT-derived signals, were digitized at a sampling rate of 2 kHz (CLAMPEX 8, Molecular Devices) in anesthetized conditions and stored in a PC. A low sampling rate (1 kHz) was used for hypoxia experiments under unanesthetized condition. A software high-pass filter (cut-off 1 Hz, CLAMPFIT 8) was used to analyse electrocardiogram, thermistor airflow sensor signal and phrenic nerve activity. A low-pass filter (cut-off 500Hz) was used for CO_2 monitoring.

Statistical analysis

Values were expressed as mean ± SE. Statistical comparison was made by unpaired or paired *t*-test using commercially available software (STATVIEW 5.0, SAS Institute, Cary, NC, USA).

Results

Gasping of knockout and wild-type mice following decapitation

In the normoxic condition, the respiratory frequency of awake Kir6.2 KO mice (3.4 ± 0.3 Hz, body weight 27.1 ± 0.4 g, n = 10) was not significantly different from that of wild-type mice (3.2 ± 0.2 Hz, body weight 26.5 ± 0.4 g, n = 12). However, when subjected to abrupt ischemia by decapitation, all wild-type mice exhibited more than 10 gasps, whereas only a very few gasps were detected in the KO mice and nine out of 20 KO mice showed no gasping at all (Fig. 3A–C). In addition to the significant difference in the number of gasps, the duration of gasping was considerably shorter in KO than in wild-type mice (Fig. 3D). In contrast, mice lacking the K_{ATP} channel subunit Kir6.1 (vascular smooth muscle-type K_{ATP} channels) exhibited gasps numbering 12.8 ± 0.3 (n = 4) with a duration of 17.3 ± 0.5 s (n = 4), not significantly different from that of wild-type mice, suggesting involvement of Kir6.2-containing K_{ATP} channels in central regulation of gasping.

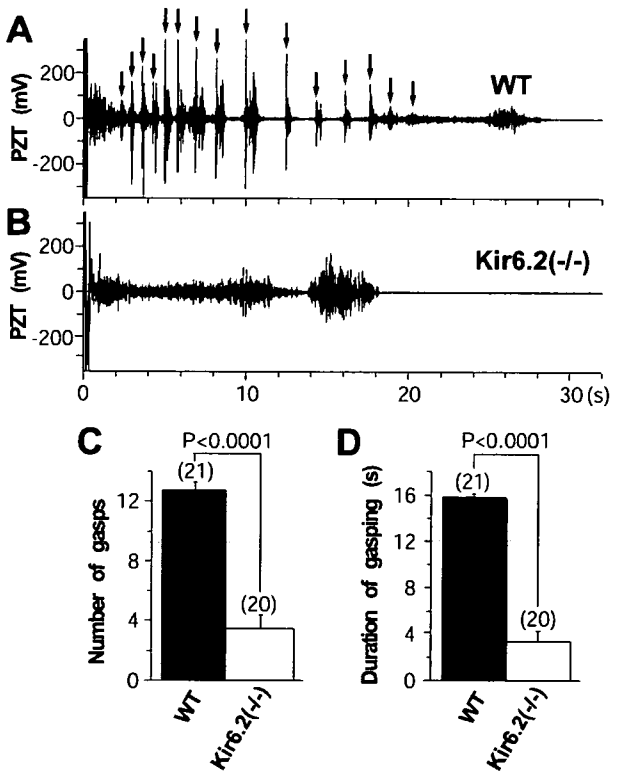

FIG. 3. Gasping caused by decapitation in wild-type (WT) and knockout (KO) mice. (A) Movement of WT head detected by piezoelectric transducer (PZT) sensor after decapitation (0 s). Arrows indicate gasping verified by video recordings (see Materials and methods). (B) Similar to A but of a KO mouse. The initial vibrations detected before 1 s after the isolation were caused by contact of the head with the PZT sensor. During this period, no gasp was observed in all mice tested. Comparison of the number (C) and total duration (D) of gasping between WT and KO mice.

Respiratory changes induced by brief hypoxia in anesthetized condition

Tachypnea and sighs

To further investigate the relevance of K_{ATP} channels in hypoxic gasping, spontaneously breathing mice were subjected under anesthesia to rapidly introduced, severe hypoxia for 60 s. This period was chosen so that both types of mice could revive after re-exposure to normoxia in the anesthetized condition. The O_2 concentration imposed on mice (5.0–5.5% measured at 60 s after introduction) was selected based on our previous study (Yamada *et al.*, 2001).

Three indices reflecting respiration were measured: changes in O_2/CO_2 concentration within the syringe connected to the tracheal cannula, changes in temperature fluctuation due to expiratory flow and respiratory body movement (Fig. 1A, see Materials and methods). Phrenic nerve activity was also monitored in some cases. However, it is known that respiratory responses to severe hypoxia are extremely sensitive to the anesthesia level and body temperature (Secher & Wilhjelm, 1968; Fewell, 2005), and the anesthesia levels of the mice subjected to phrenic nerve recordings were difficult to keep equalized during the hypoxia experiment. Accordingly, traces of phrenic nerve recordings were selected to represent typical hypoxic responses (Fig. 4A and B).

The initial responses of wild-type mice, along with a rapidly declining O_2 concentration, were augmented respiratory frequency (tachypnea, Fig. 4, A1 and A2, onset indicated by open arrowhead) and a subsequent extraordinarily large breath (asterisks in Fig. 4, A1). The large breath, referred to as a sigh, was easily identified by its biphasic large deflection in the trace of the thermistor airflow sensor. As indicated by the concomitant increase in expired CO_2 (Figs 4, A1, and 5, A1), these deflections reflect the large-amplitude expiration of a sigh (see later sections for details).

The onset of tachypnea and initial sigh were similar in wild-type and KO mice (Figs 4, A1–C1, and 6, A1 and B1). However, the maximal respiratory frequency during tachypnea was higher and the peak period of tachypnea (from onset to maximum tachypnea) was longer in KO than in wild-type mice (Figs 4, A2–C2, 5, A1 and B1, and 6, A2 and A3). In addition, most (10/12) KO mice exhibited an apnea-like period (duration 13.3 ± 1.4 s, onset 26.9 ± 1.0 s, n = 10) following tachypnea (Figs 4, C1 and C2, and 5C). During this apnea-like period, the respiratory frequency may have been too high, as indicated by the PZT deflections, for these breaths to be detected by thermistor or CO_2 sensor (Fig. 5C). Accordingly, the apnea-like periods were not counted as depression in the anesthetized experiment. No such apnea-like period was detected in the wild-type mice tested (n = 23) during the 60-s hypoxic period.

Depression in respiratory frequency

Following the tachypnea, the respiratory frequency of wild-type mice was quickly depressed to a value below the mean frequency before hypoxia (depression, after filled arrow in Fig. 4, A2). In addition, the amplitude of CO_2 and thermistor airflow sensor traces progressively

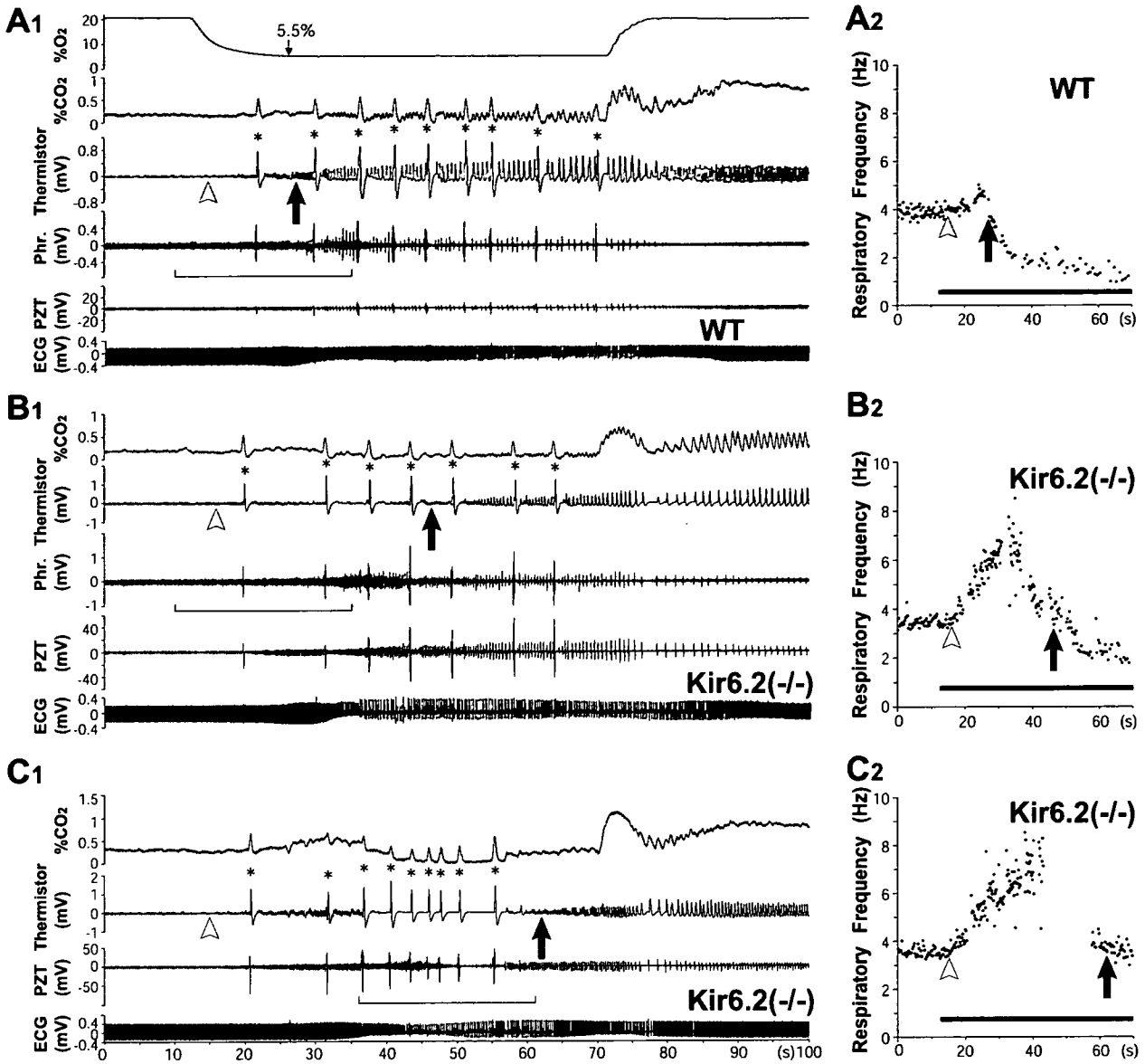

FIG. 4. Brief hypoxia (60 s)-induced respiration changes in mice under anesthesia. (A1) Representative responses of a wild-type (WT) mouse. Electromagnetic three-way valve for introducing hypoxic gas was opened at 10 s (the time lag in percentage O_2 change was due to dead volume in the gas inlet tube and syringe). At 60 s after valve opening, percentage O_2 in the syringe reached 5.0% (the time at 5.5% O_2 is indicated). Delay originating from the response time of the O_2/CO_2 gas analyser (~7.5 s) was corrected. An increase in percentage CO_2 reflects expiratory outflow from the tracheal cannula. Temperature increase due to expiratory flow was monitored by a thermistor airflow sensor (Thermistor; see Materials and methods). Biphasic large deflections in the trace of the thermistor (asterisks) are referred to as 'sighs'. Onsets of tachypnea and depression are indicated by open arrowhead and filled arrow, respectively. Operation for phrenic nerve recording (Phr.) in this mouse minimally affected the response. Inspiratory and expiratory body movement were monitored by piezoelectric transducer (PZT) deflections in the opposite direction. Electrocardiogram (ECG) was monitored. The underlined period is expanded in Fig. 5A to show details in the initial hypoxic responses. (B1) Similar to A1 but of a knockout (KO) mouse. (C1) Similar to B1 but of another KO mouse showing apnea-like period interrupted by sighs. Phrenic recording was not conducted in this case. Detail in the responses during the apnea-like period (underlined) is shown in Fig. 5C. (A2) Change in respiratory frequency of WT mouse shown in A1. Filled bar denotes period of actual hypoxic challenge. Open arrowhead and filled arrow indicate the onset of tachypnea and depression, respectively (see Materials and methods). (B2 and C2) Similar to A2 but of KO mice shown in B1 and C1, respectively. In the brief hypoxia experiment, thermistor sensor responses were used to count frequency and sighs were not counted. Hence, the trace in C2 shows an intermittent period after tachypnea.

increased, indicating increased tidal volume during depression (Figs 4, A1, and 5, A1). The frequency slowed further to below 2 Hz in a short period, while a large tidal volume was maintained (Figs 4, A1 and A2, and 5, A1). Based only on the tidal volume and interbreath interval, the slow respiration during this period (frequency <~2Hz) may be regarded as gasping. With regard to phrenic nerve activity, the burst of gasping in small animals such as mice has been characterized by its larger amplitude and shorter duration compared with those in eupnea, in addition to a long intergasp interval (St. John & Paton, 2003). However, the amplitude of the phrenic bursts in wild-type mice during this slow respiration period was frequently not much larger (Fig. 4, A1, see the trace of phrenic activity) than that during eupnea and the duration of the burst was long in some instances (see also Fig. 8, A2), making it difficult to determine if such slow respiration is gasping or depression.

Although KO mice also showed a depression similar to that seen in wild-type mice, its onset was significantly delayed (Figs 4B and C, and 6C). Thus, tachypnea was more quickly depressed in wild-type

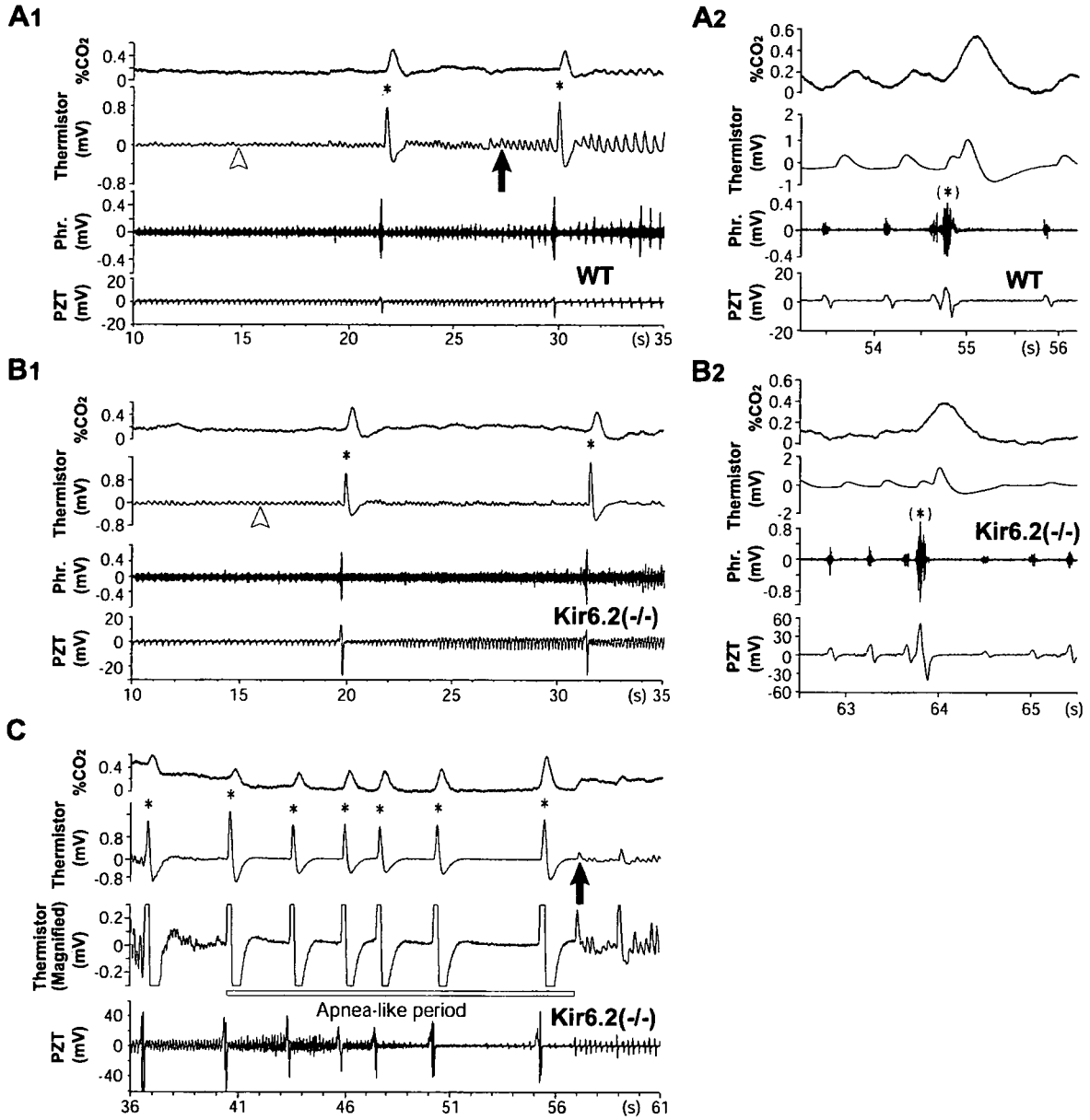

FIG. 5. Details in respiratory responses during brief hypoxia. (A1) Initial hypoxic responses of a wild-type (WT) mouse underlined in Fig. 4A1. Onsets of tachypnea (open arrowhead) and depression (filled arrow) are indicated in the thermistor trace. Asterisks denote sighs (as in Fig 4). (B1) Similar to A1 but of a knockout (KO) mouse underlined in Fig. 4B1. (A2 and B2) Phrenic nerve discharges corresponding to sighs (asterisks in parenthesis) of WT and KO mice in A1 and B1, respectively. To show the phrenic discharge pattern, these sighs were chosen from the later period when sighs emerged independently of neighboring breaths, as the initial sighs in A1 and B1 during tachypnea overlapped to a variable extent with neighboring fast breaths. Simultaneous recordings of phrenic nerve activity and piezoelectric transducer (PZT) responses demonstrate that the upward deflection in the PZT trace correlated well with the phrenic burst, i.e. the inspiratory activity. The response time-lag in percentage CO_2 was corrected as in Fig. 4. As other traces are shown in real time, the thermistor responses are shown slightly delayed from phrenic discharges and PZT responses. (C) Details in apnea-like period after tachypnea underlined in Fig. 4C1. The thermistor response in the second trace is redrawn in the third trace at a magnified scale to demonstrate that breaths between sighs were undetectable by the thermistor sensor. As the PZT sensor is extremely sensitive, very fast breathing-like motions were detected between sighs in the initial stage of the apnea-like period. Phr., phrenic nerve recording.

than in KO mice in the anesthetized condition. A similar further slowing of respiration (< 2 Hz) was also observed in some KO mice within the brief hypoxic period (Fig. 4, B2).

Characterization of sighs during brief hypoxia

The extraordinary large-amplitude breaths termed here as sighs are characterized by phrenic nerve discharge with an amplitude much larger than that of a eupneic breath (Fig. 4, see also Fig. 5, A2 and B2). In addition, a sigh was clearly distinguishable from neighboring breaths by the deeper and wider downward deflections seen in the trace of the thermistor airflow sensor (Fig. 4A–C), indicating that sighs involve expiration of larger amplitude and longer duration (see Materials and methods). In addition, sighs emerged independently of the neighboring breaths (Fig. 5, A2 and B2, asterisks) and were followed by a short duration post-sigh apneic period (Nakamura *et al.*, 2003).

When the number of sighs was counted on this definition, the onset and number of sighs were similar in wild-type and KO mice, except

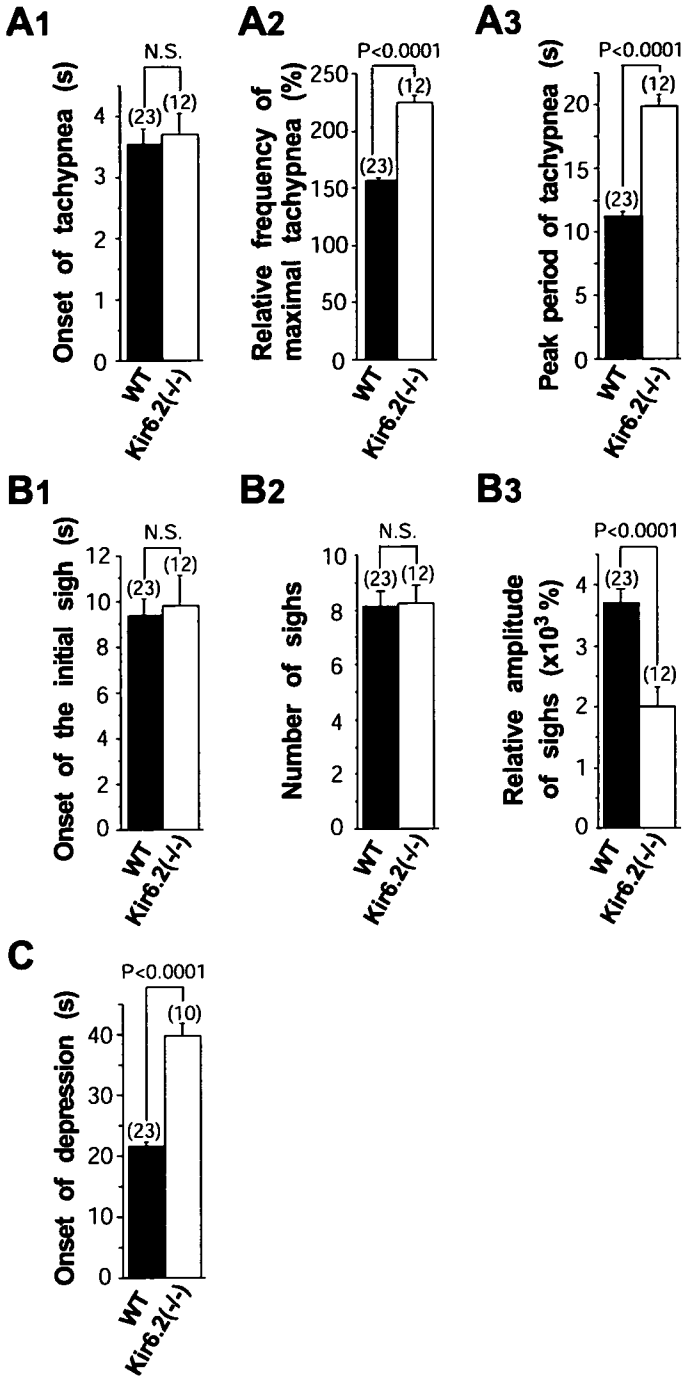

FIG. 6. Comparison of brief hypoxia-induced respiratory changes between wild-type (WT) and knockout (KO) mice. (A1, A2 and A3) The onset, maximal respiratory frequency relative to the mean frequency before hypoxic challenge and peak period (time from onset to maximum) of tachypnea, respectively. (B1 and B2) Onset and the number of sighs. (B3) The mean amplitude of sighs relative to that of breaths before hypoxic challenge evaluated by thermistor sensor. (C) Onset of depression. Two KO mice did not show depression during the 60-s hypoxic period. Onsets in all figures were measured from the time that the O_2 concentration actually began to decrease (see Fig. 4A1). N.S., not significant.

that the mean amplitude of sighs relative to that of eupneic breaths was lower in KO than in wild-type mice (Fig. 6, B1–B3). These results suggest that K_{ATP} channels are not required in the generation and maintenance of sighs.

Respiratory changes in prolonged hypoxia in anesthetized condition

The brief hypoxia experiment suggested investigation of respiratory changes during a longer hypoxic period. We then examined the effect of prolonged hypoxia in the anesthetized condition while recording phrenic nerve activity, introduced as in the brief hypoxia experiment (to 5.0% O_2 in 60 s) and maintained until cessation. As the hypoxic period was longer, the O_2 concentration finally reached nearly the value of the pre-mixed gas (4.5% O_2) (see Materials and methods).

In wild-type mice, tachypnea, sighs and depression were elicited during the initial 60-s hypoxia in a manner essentially similar to that described in previous sections (Figs 7 and 10A). However, after this period, the sighs ceased and the basal respiratory frequency became gradually slower, stabilizing at a very low frequency (< ~0.5 Hz), which persisted for tens of seconds (Figs 7A and 9, A1). The PZT signal during this stable phase exhibited a biphasic symmetrical shape (Fig. 8, A3, bottom trace), whereas in the eupneic period the shape was asymmetrical, with upward deflection of less amplitude and longer duration than the subsequent downward deflection (Fig. 8, A1). In the depression period preceding this stable phase, the PZT signal also exhibited an asymmetrical shape in the beginning but gradually shifted to symmetrical (Figs 7A, and 8, A2 and A3). To quantify the symmetry of the PZT shape, we used a shape index in the present study that becomes closer to 1 as the PZT shape becomes more symmetrical (see Materials and methods).

As shown in Fig. 9, B1, the shape index during the initial phase of depression in wild-type mice fluctuated greatly but the value soon became stable at a value close to 1. The shape index clearly shows a stable respiration phase of some duration after the onset of depression (open arrow in Fig. 9, B1). From this point, respiratory body movement detected by PZT shifted to biphasic symmetrical, reflecting an inspiration followed by an expiration involving an almost equal amount of vertical motion. Thus, a PZT shape index that became stable at a value close to 1 (ranging from 0.4 to 2.0) was termed persistent gasping. The duration of the depression in respiratory frequency was then counted as the period from its onset (filled arrow in Fig. 9, A1, when the respiratory frequency after tachypnea first decreased to a value less than the mean frequency before hypoxia) until the onset of persistent gasping (open arrow in Fig. 9, B1).

After the onset of depression (filled arrow in Fig. 9, A1), the width of the phrenic burst also decreased gradually in wild-type mice (Fig. 9, C1) but some fluctuation was still seen. In contrast, during persistent gasping, the phrenic burst showed a stable value that was significantly shorter (0.06 ± 0.00 s, $n = 4$) than during eupnea (0.11 ± 0.09 s, $n = 4$, $P < 0.005$, paired t-test; Figs 8, A1 and A3, and 9, C1), indicating that breathing during persistent gasping meets at least one of the conventional criteria of gasping, a shorter duration of phrenic burst than in eupnea, although the amplitude of the burst was not always much larger than in eupnea (see also Fig. 7A).

In KO mice, depression in respiratory frequency could be detected (Figs 7B, 8B and 9, A2) but its onset was delayed by ~15 s and its duration was shorter by ~80 s than in wild-type mice (Fig. 10A, see also Fig. 6C). As a consequence, the onset of persistent gasping in KO mice was significantly earlier than in wild-type mice (Figs 9, B1 and B2, and 10, B1).

When the hypoxic condition was continued further, the stable period of persistent gasping in wild-type mice stopped abruptly with a dramatic increase in the width of the phrenic burst, whereupon respiration ceased (Figs 7A and 8, A4; after thin arrow in Fig. 9, C1). The mean width of the phrenic bursts of the last four gasps except for the very last one of the terminal breaths was significantly wider

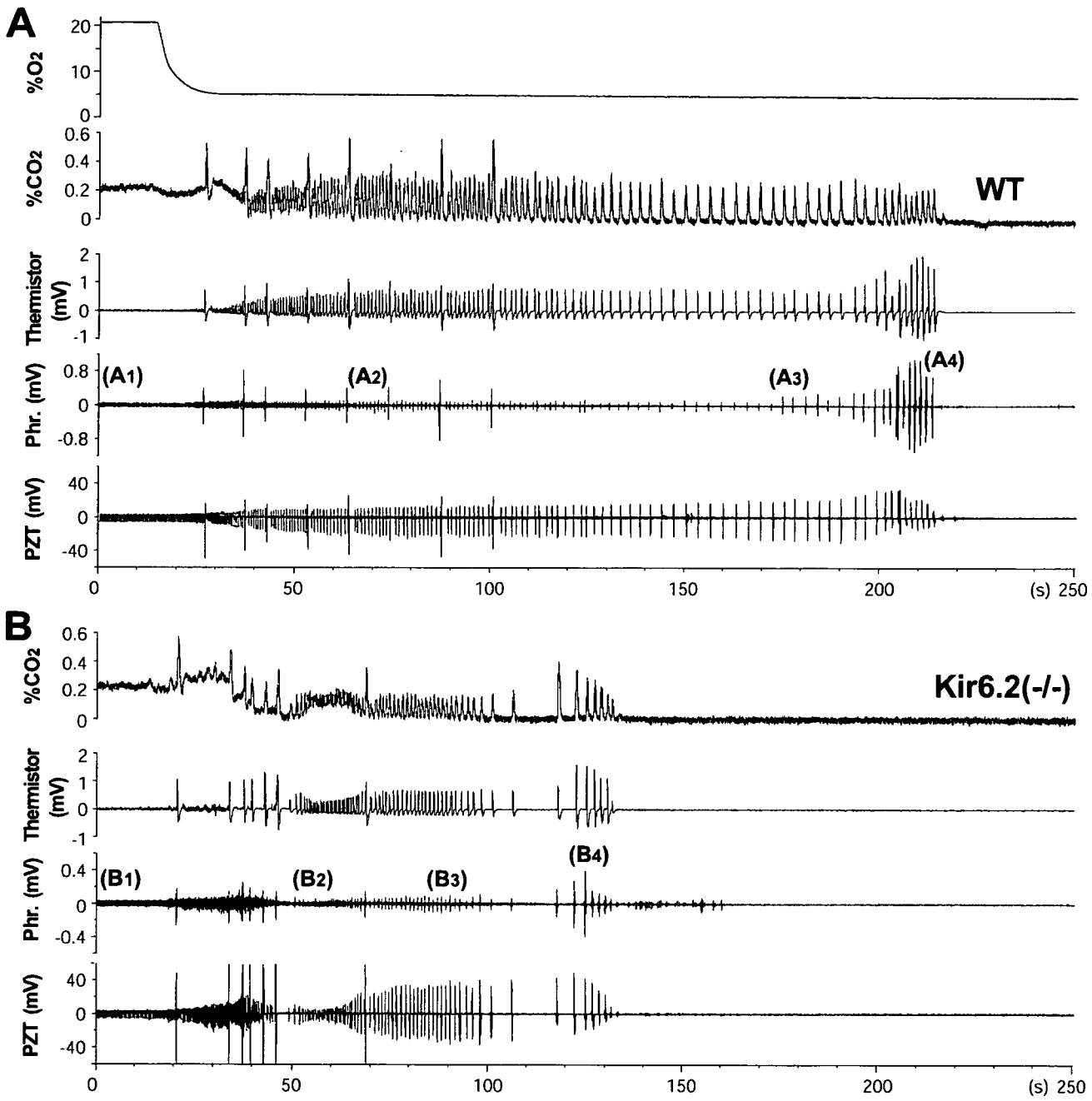

FIG. 7. Changes in respiration of wild-type (WT) (A) and knockout (KO) (B) mice subjected to hypoxia in a similar manner to the brief hypoxia (5.0% O_2 at 60 s) in anesthetized condition but for a more prolonged period. (A) Following the initial 60 s from hypoxia onset, stable, very slow respiration persisted until the emergence of several terminal breaths of large expiratory flow similar to the sighs seen in the thermistor trace but exhibiting a much wider phrenic burst than that of sighs. (B) Similar to A but of a KO mouse. Apnea-like periods are seen after tachypnea and before the terminal breaths. Responses marked by A1–4 and B1–4 in parenthesis are shown magnified in Fig. 8.

(0.33 ± 0.02 s, $n = 4$) than that of phrenic bursts during persistent gasping (0.06 ± 0.00 s, $n = 4$; $P < 0.005$, paired t-test). Thus, breathing after the time point at which the width of the phrenic burst showed an abrupt increase (thin arrow in Fig. 9, C1) was termed terminal gasping and persistent gasping continued until the onset of terminal gasping in the anesthetized experiment.

Corresponding to the large width of phrenic bursts in terminal gasping, which indicates a large inspiration, the duration between positive and negative PZT deflections was long, i.e. movement during expiration showed a delayed peak (Fig. 8, A4, downward deflections in the bottom trace). Indeed, the time point at which the width of the phrenic burst began to increase (Fig. 9, C1, thin arrow) correlated well with the shape index of the PZT falling close to 0 (Fig. 9, B1 and C1), reflecting an increase in the duration of individual expiratory flow, especially very close to the baseline (Fig. 8, A4). In addition, the amplitude of the downward deflections in the trace of the thermistor airflow sensor during terminal gasping was as large as that of sighs (Fig. 7A, third trace), also suggesting a long duration and large amplitude expiratory breath of terminal gasping as mentioned in the analysis of sighs above. The long duration of the individual expirations was most clearly seen in the PZT traces in some wild-type and KO mice (Fig. 8, B4, bottom trace).